November 2004

Symmetries, inversion formulas, and image reconstruction for optical tomography

Vadim A. Markel
University of Pennsylvania

John C. Schotland
University of Pennsylvania, schotland@seas.upenn.edu

Copyright American Physical Society. Reprinted from *Physical Review E*, Volume 70, Issue 5, Article 056616, November 2004, 19 pages.
Publisher URL: http://dx.doi.org/10.1103/PhysRevE.70.056616

Symmetries, inversion formulas, and image reconstruction for optical tomography

Abstract

We consider the image reconstruction problem for optical tomography with diffuse light. The associated inverse scattering problem is analyzed by making use of particular symmetries of the scattering data. The effects of sampling and limited data are analyzed for several different experimental modalities, and computationally efficient reconstruction algorithms are obtained. These algorithms are suitable for the reconstruction of images from very large data sets.

Publisher URL: http://dx.doi.org/10.1103/PhysRevE.70.056616

Symmetries, inversion formulas, and image reconstruction for optical tomography

Vadim A. Markel*
Department of Radiology, University of Pennsylvania, Philadelphia, Pennsylvania 19104, USA

John C. Schotland†
Department of Bioengineering, University of Pennsylvania, Philadelphia, Pennsylvania 19104, USA
(Received 14 June 2004; published 30 November 2004)

We consider the image recostruction problem for optical tomography with diffuse light. The associated inverse scattering problem is analyzed by making use of particular symmetries of the scattering data. The effects of sampling and limited data are analyzed for several different experimental modalities, and computationally efficient reconstruction algorithms are obtained. These algorithms are suitable for the reconstruction of images from very large data sets.

DOI: 10.1103/PhysRevE.70.056616 PACS number(s): 42.30.Wb, 41.20.Jb, 42.62.Be

I. INTRODUCTION

A. Review of the problem

There has been considerable recent interest in the development of optical methods for biomedical imaging [1–5]. The near-IR spectral region is of particular importance for such applications in view of the presence of a "window of transparency" in the absorption spectrum of biological tissues between 700 and 900 nm. However, the propagation of near-IR light in tissue is characterized by strong multiple scattering which renders traditional imaging methods based on ray optics invalid. Imaging modalities which utilize multiply scattered light in the diffusion regime are referred to as optical diffusion tomography (ODT).

The propagation of electromagnetic radiation in strongly scattering media can be described by the radiative transport equation (RTE) or by the diffusion equation (DE) [6,7]. In both approaches, information about the phase of the electromagnetic wave is lost and the transport of light is characterized by the specific intensity $I(\mathbf{r},\hat{\mathbf{s}})$ at the point $\mathbf{r}$ flowing in the direction $\hat{\mathbf{s}}$. This description relies on a fundamental assumption — namely, that the intensity rather than the amplitude of the radiation field satisfies the superposition principle. An important consequence of this fact is that the specific intensity may be expressed in terms of the Green's function of an appropriate differential or integro-differential equation according to

$$I(\mathbf{r},\hat{\mathbf{s}}) = \int G(\mathbf{r},\hat{\mathbf{s}};\mathbf{r}',\hat{\mathbf{s}}')\varepsilon(\mathbf{r}',\hat{\mathbf{s}}')d^3r'd^2\hat{s}', \tag{1}$$

where $\varepsilon(\mathbf{r},\hat{\mathbf{s}})$ is an appropriate source function and we have assumed that the specific intensity is stationary in time.

In a typical experiment, light is injected into an inhomogeneous medium by one or more optical fibers which act as point sources. Additional fibers are employed for collection and subsequent detection of the transmitted light. Thus, if a source is located at the point $\mathbf{r}_s$ and produces a narrow collimated incident beam in the direction $\hat{\mathbf{s}}_s$ and the detector measures the specific intensity at the point $\mathbf{r}_d$ flowing in the direction $\hat{\mathbf{s}}_d$, the measurable quantity (up to a multiplicative constant proportional to the total power of the source and the efficiency of the detector) is the Green's function $G(\mathbf{r}_s,\hat{\mathbf{s}}_s;\mathbf{r}_d,\hat{\mathbf{s}}_d)$. Reconstructing the optical properties of the medium from measurements of $G(\mathbf{r}_s,\hat{\mathbf{s}}_s;\mathbf{r}_d,\hat{\mathbf{s}}_d)$ constitutes the inverse problem of ODT.

The formulation of the inverse problem of ODT is based on the fact that G may be related to the optical properties of the medium. This dependence is nonlinear [8], which significantly complicates the inverse problem. Indeed, the Dyson equation for G can be written in operator form as

$$G = G_0 - G_0VG, \tag{2}$$

where G_0 is the Green's function for a homogeneous medium and V is the operator which describes the deviations of the optical properties of the medium from their background values. From the relation $G=(1+G_0V)^{-1}G_0$, it can be seen that G is a nonlinear functional of V. It is possible to linearize the inverse problem under the assumption that V is small, as is the case in many physical applications [9]. The simplest approach is to use the first Born approximation which is given by

$$G = G_0 - G_0VG_0. \tag{3}$$

In this case the main equation of ODT can be formulated as

$$\Phi = G_0VG_0, \tag{4}$$

where $\Phi=G_0-G$ is the experimentally measurable data function. Note that other methods of linearization can also be used, leading to an equation of the form (4) with a modified expression for Φ (see Sec. II below).

Since the right-hand side of Eq. (4) contains only the unperturbed Green's function G_0, the properties of G_0 are of primary importance. Although the functional form of G_0 can be quite complicated, as in the case of the RTE, some useful relations may be obtained from the underlying symmetry of the problem. In a recent series of papers [10–14] we have

*Electronic address: vmarkel@mail.med.upenn.edu
†Electronic address: schotland@seas.upenn.edu

exploited the translational invariance of the unperturbed medium in the slab measurement geometry within the diffusion approximation. Several reconstruction algorithms have been proposed and numerically simulated. It was shown that taking into account translational invariance can result in a dramatic improvement of computational performance. In particular, it allows the reconstruction of data sets with a very large number of source detector pairs, a situation in which numerical reconstruction methods cannot be used due to their high computational complexity. In Refs. [12,13] the effects of sampling and limited data were studied and it was shown that the fundamental limit of transverse resolution is given by the step size of the lattice on which sources or detectors are placed. Therefore, a large number of source-detector pairs is required to achieve the highest possible spatial resolution.

Although the methods discussed in Refs. [10–14] may appear to be distinctly different, they are, in fact, special cases of a general family of inversion formulas which are based on certain symmetries of the unperturbed medium. The derivation of these results is, in some sense, independent of the use of the diffusion approximation. Indeed, the only important property of the Green's function G_0 which is used is translational or rotational invariance. In a general curvilinear system of orthogonal coordinates x_1, x_2, x_3 invariance with respect to translation of one of the coordinates—say, x_1—can be mathematically expressed as $G_0(x_1, x_2, x_3; x_1', x_2', x_3') = f(x_1 - x_1'; x_2, x_3; x_2', x_3')$ for some function f. Geometries in which translational invariance exists with respect to two coordinates are of particular interest. For example, in the slab measurement geometry discussed in Sec. III, G_0 is invariant with respect to translations parallel to the measurement plane; in the cylindrical measurement geometry which is discussed in Sec. V, G_0 is invariant with respect to rotations about and translations parallel to the cylinder axis.

Apart from generalizations of previously obtained results and placing them in a unified theoretical framework, this paper contains the following new developments.

(i) We have shown that symmetry-based image reconstruction methods are applicable not only to the DE but to the more general RTE. An example of an integral kernel derived from the RTE has been given.

(ii) A novel method (applicable to both DE and RTE) of linearization of the inverse problem has been proposed.

(iii) The case when the sources and detectors are placed on different lattices or when only the sources are placed on a lattice is consistently treated.

(iv) A multiprojection imaging scheme is proposed in which data from multiple rotations of a slab are used self-consistently.

B. Green's functions in radiative transport and diffusion theory

We assume that all sources are harmonically modulated at a frequency ω, typically in the radio-frequency range (not to be confused with the electromagnetic frequency). This includes continuous-wave (cw) experiments with $\omega = 0$ as a special case. In general, all time-dependent quantities acquire the usual factor $\exp(-i\omega t)$, and the RTE in the frequency domain can be written as

$$[\hat{\mathbf{s}} \cdot \nabla + (\mu_a + \mu_s - i\omega/c)] I(\mathbf{r}, \hat{\mathbf{s}}) - \mu_s \int A(\hat{\mathbf{s}}, \hat{\mathbf{s}}') I(\mathbf{r}, \hat{\mathbf{s}}') d^2\hat{s}' = \varepsilon(\mathbf{r}, \hat{\mathbf{s}}), \tag{5}$$

where μ_a and μ_s are the absorption and scattering coefficients, c is the average speed of light in the medium, and $A(\hat{\mathbf{s}}, \hat{\mathbf{s}}')$ is the scattering kernel (also known as the phase function) with the properties $A(\hat{\mathbf{s}}, \hat{\mathbf{s}}') = A(\hat{\mathbf{s}}', \hat{\mathbf{s}})$ and $\int A(\hat{\mathbf{s}}, \hat{\mathbf{s}}') d^2\hat{s}' = 1$ for all $\hat{\mathbf{s}}$.

In radiative transport theory, it is customary to distinguish the diffuse and reduced specific intensities I_d and I_r. The latter can be defined in several different ways, which, in turn, influences the definition of I_d. The DE is obtained most naturally if the reduced intensity is chosen so that

$$[\hat{\mathbf{s}} \cdot \nabla + (\mu^* - i\omega/c)] I_r = \varepsilon(\mathbf{r}, \hat{\mathbf{s}}), \tag{6}$$

where $\mu^* = \mu_a + (1-g)\mu_s$, $g = \int (\hat{\mathbf{s}} \cdot \hat{\mathbf{s}}') A(\hat{\mathbf{s}} \cdot \hat{\mathbf{s}}') d^2 s$ is the scattering asymmetry parameter, and the boundary conditions at the surface $\partial\Omega$ where the incident radiation with specific intensity I_{inc} enters the scattering medium is $I_r|_{\mathbf{r} \in \partial\Omega} = I_{\text{inc}}$. Then the diffuse intensity I_d satisfies

$$[\hat{\mathbf{s}} \cdot \nabla + (\mu^* - i\omega/c)] I_d(\mathbf{r}, \hat{\mathbf{s}}) - \mu_s' \int A'(\hat{\mathbf{s}}, \hat{\mathbf{s}}') I_d(\mathbf{r}, \hat{\mathbf{s}}') d^2\hat{s}' = \varepsilon_r(\mathbf{r}, \hat{\mathbf{s}}), \tag{7}$$

where $\mu_s' = (1-g)\mu_s$ is the reduced scattering coefficient and $A'(\hat{\mathbf{s}}, \hat{\mathbf{s}}') = [A(\hat{\mathbf{s}}, \hat{\mathbf{s}}') - g\delta(\hat{\mathbf{s}} - \hat{\mathbf{s}}')]/(1-g)$, and the source term due to the reduced intensity, $\varepsilon_r(\mathbf{r}, \hat{\mathbf{s}})$, is given by

$$\varepsilon_r(\mathbf{r}, \hat{\mathbf{s}}) = \mu_s' \int A'(\hat{\mathbf{s}}, \hat{\mathbf{s}}') I_r(\mathbf{r}, \hat{\mathbf{s}}') d^2\hat{s}'. \tag{8}$$

Note that the modified scattering kernel $A'(\hat{\mathbf{s}}, \hat{\mathbf{s}}')$ is still normalized by the condition $\int A'(\hat{\mathbf{s}}, \hat{\mathbf{s}}') d^2 s = 1$, but the first moment (asymmetry factor) $\int (\hat{\mathbf{s}} \cdot \hat{\mathbf{s}}') A'(\hat{\mathbf{s}}, \hat{\mathbf{s}}') d^2 s$ is identically zero. We will assume everywhere below that the ballistic component of the intensity given by I_r at the location of detectors is negligibly small and will focus on the diffuse component descried by Eq. (7).

An inhomogeneous medium is characterized by the spatial distribution $\mu_a(\mathbf{r}) = \mu_{a0} + \delta\mu_a(\mathbf{r})$ and $\mu_s(\mathbf{r}) = \mu_{s0} + \delta\mu_s(\mathbf{r})$. Alternatively, we can consider the variables $\mu^*(\mathbf{r}) = \mu_0^* + \delta\mu^*(\mathbf{r})$ and $\mu_s'(\mathbf{r}) = \mu_{s0}' + \delta\mu_s'(\mathbf{r})$ as mathematically independent. In particular, if only μ_a varies (the case of absorbing inhomogeneities), the quantity μ^* is also varying while μ_s' is constant. The Green's function for the RTE, $G(\mathbf{r}, \hat{\mathbf{s}}; \mathbf{r}', \hat{\mathbf{s}}')$, satisfies the Dyson equation (2) with the operator V given by $V = \delta\mu^* - \delta\mu_s' A'$. The operator A' with matrix elements $\langle \mathbf{r}\hat{\mathbf{s}} | A' | \mathbf{r}'\hat{s}' \rangle = \delta(\mathbf{r} - \mathbf{r}') A'(\hat{\mathbf{s}}, \hat{\mathbf{s}}')$ is assumed to be position independent. The unperturbed Green's function $G_0(\mathbf{r}, \hat{\mathbf{s}}; \mathbf{r}', \hat{\mathbf{s}}')$ satisfies

$$[\hat{\mathbf{s}}\cdot\nabla+(\mu_0^*-i\omega/c)]G_0(\mathbf{r},\hat{\mathbf{s}};\mathbf{r}',\hat{\mathbf{s}}')-\mu_{s0}'\int A'(\hat{\mathbf{s}},\hat{\mathbf{s}}'')G_0(\mathbf{r},\hat{\mathbf{s}}'';\mathbf{r}',\hat{\mathbf{s}}')d^2\hat{s}''=\delta(\mathbf{r}-\mathbf{r}')\delta(\hat{\mathbf{s}}-\hat{\mathbf{s}}'). \tag{9}$$

The DE is obtained by expanding $I_d(\mathbf{r},\hat{\mathbf{s}})$ to first order in $\hat{\mathbf{s}}$ (for nonzero modulation frequencies, an additional condition $\omega\ll\mu^* c$ must be fulfilled):

$$I_d(\mathbf{r},\hat{\mathbf{s}})=\frac{c}{4\pi}u+\frac{3}{4\pi}\mathbf{J}\cdot\hat{\mathbf{s}}, \tag{10}$$

where

$$u(\mathbf{r})=\frac{1}{c}\int I_d(\mathbf{r},\hat{\mathbf{s}})d^2\hat{s},\quad \mathbf{J}(\mathbf{r})=\int\hat{\mathbf{s}}I_d(\mathbf{r},\hat{\mathbf{s}})d^2\hat{s}. \tag{11}$$

Then the density of electromagnetic energy u satisfies

$$-\nabla\cdot[D(\mathbf{r})\nabla u(\mathbf{r})]+[\alpha(\mathbf{r})-i\omega]u(\mathbf{r})=S(\mathbf{r}) \tag{12}$$

and the current $\mathbf{J}$ is given by

$$\mathbf{J}=-D\nabla u, \tag{13}$$

where $D=c/3\mu^*$ and $\alpha=c\mu_a$ are the diffusion and absorption coefficients, and

$$S(\mathbf{r})=\int\varepsilon_r(\mathbf{r},\hat{\mathbf{s}})d^2\hat{s} \tag{14}$$

is the source for the DE. Note that the specific choice of the reduced intensity (6) has resulted in a simple form for the source function S which does not contain higher moments of ε_r (compare with the analogous formulas in [6]).

The Green's function for the DE does not depend on the directions $\hat{\mathbf{s}}$ and $\hat{\mathbf{s}}'$, and we denote its matrix elements by $G(\mathbf{r},\mathbf{r}')$. The Green's function of the RTE for the diffuse component of specific intensity can be related to $G(\mathbf{r},\mathbf{r}')$ by applying the formula (10) to the electromagnetic energy density $u(\mathbf{r})=\int G(\mathbf{r},\mathbf{r}')S(\mathbf{r}')d^3r'$. For a point unidirectional source $\varepsilon(\mathbf{r},\hat{\mathbf{s}})=\delta(\mathbf{r}-\mathbf{r}_0)\delta(\hat{\mathbf{s}}-\hat{\mathbf{s}}_0)$ and homogeneous boundary conditions $I_{\text{inc}}=0$ one can easily find that

$$S(\mathbf{r})=\mu_s'\Theta(\hat{\mathbf{s}}_0\cdot(\mathbf{r}-\mathbf{r}_0))\exp[-\mu^*\hat{\mathbf{s}}_0\cdot(\mathbf{r}-\mathbf{r}_0)]\delta(\mathbf{r}-\hat{\mathbf{s}}_0(\hat{\mathbf{s}}_0\cdot\mathbf{r})-\mathbf{r}_0+\hat{\mathbf{s}}_0(\hat{\mathbf{s}}_0\cdot\mathbf{r}_0)), \tag{15}$$

where $\Theta(x)$ is the step function and we have used the condition $\omega\ll\mu^* c$.

Note that the same expression for $S(\mathbf{r})$ is obtained by assuming that there are no internal sources ($\varepsilon=0$) and using the inhomogeneous boundary conditions $I_r|_{\mathbf{r}\in\partial\Omega}=I_{\text{inc}}$ where I_{inc} is the intensity of a collimated narrow beam entering the medium at the point $\mathbf{r}_0\in\partial\Omega$ in the incident direction $\hat{\mathbf{s}}_0$. By expanding the diffuse Green's function near the point $\mathbf{r}'=\mathbf{r}_0$ according to $G(\mathbf{r},\mathbf{r}')=G(\mathbf{r},\mathbf{r}_0)+(\mathbf{r}'-\mathbf{r}_0)\cdot\nabla_{\mathbf{r}'}G(\mathbf{r},\mathbf{r}')|\mathbf{r}'=\mathbf{r}_0$ and using Eq. (10) the RTE Green's function for the diffuse component can be expressed in terms of the DE Green's function as

$$G(\mathbf{r},\hat{\mathbf{s}};\mathbf{r}',\hat{\mathbf{s}}')=\frac{c\mu_s'\ell^*}{4\pi}(1+\ell^*\hat{\mathbf{s}}\cdot\nabla_{\mathbf{r}})(1-\ell^*\hat{\mathbf{s}}'\cdot\nabla_{\mathbf{r}'})G(\mathbf{r},\mathbf{r}'), \tag{16}$$

where

$$\ell^*\equiv 1/\mu^*=3D_0/c. \tag{17}$$

Note that Eq. (16) satisfies the general reciprocity relation $G(\mathbf{r},\hat{\mathbf{s}};\mathbf{r}',\hat{\mathbf{s}}')=G(\mathbf{r}',-\hat{\mathbf{s}}';\mathbf{r},-\hat{\mathbf{s}})$ [15].

The DE (12) must be supplemented with boundary conditions which, in the general case, have the form

$$(u+\ell\hat{\mathbf{n}}\cdot\nabla u)|_{\mathbf{r}\in\partial\Omega}=0, \tag{18}$$

where ℓ is the *extrapolation distance* [16] and $\hat{\mathbf{n}}$ is an outward unit normal to the surface, $\partial\Omega$, at the point $\mathbf{r}$. If we assume that $\mathbf{r}_s,\mathbf{r}_d\in\partial\Omega$, expression (16) can be simplified with the use of Eq. (18), which $G(\mathbf{r},\mathbf{r}')$ must satisfy with respect to both of its arguments. Namely, if the source and detector optical fibers are oriented perpendicular to the measurement surface, we have $\hat{\mathbf{s}}\cdot\hat{\mathbf{n}}=-1$ for the source and $\hat{\mathbf{s}}'\cdot\hat{\mathbf{n}}'=1$ for the detector. Consequently, Eq. (16) takes the form

$$G(\mathbf{r},\hat{\mathbf{s}};\mathbf{r}',\hat{\mathbf{s}}')|_{\mathbf{r},\mathbf{r}'\in\partial\Omega}=\frac{c\mu_s'\ell^*}{4\pi}\left(1+\frac{\ell^*}{\ell}\right)^2G(\mathbf{r},\mathbf{r}'). \tag{19}$$

Thus, the Green's function for the RTE has been expressed in terms of the Green's function for the DE and the parameters ℓ and ℓ^*. Note that in the limit $\ell\to 0$ (purely absorbing boundaries), the quantity on the right-hand side of Eq. (19) is finite since $G(\mathbf{r},\mathbf{r}')$ goes to zero as ℓ^2 for $\mathbf{r},\mathbf{r}'\in\partial\Omega$.

Inhomogeneities of the medium are described in the DE by spatial fluctuations of the absorption and diffusion coefficients: $\alpha(\mathbf{r})=\alpha_0+\delta\alpha(\mathbf{r})$ and $D(\mathbf{r})=D_0+\delta D(\mathbf{r})$. The unperturbed Green's function satisfies

$$(-D_0\nabla^2+\alpha_0-i\omega)G_0(\mathbf{r},\mathbf{r}')=\delta(\mathbf{r}-\mathbf{r}'), \tag{20}$$

and the full Green's function G satisfies the Dyson equation (2) with the interaction operator given by

$$V=\delta\alpha(\mathbf{r})-\nabla\cdot\delta D(\mathbf{r})\nabla. \tag{21}$$

The remainder of this paper is organized as follows. In Sec. II several methods for the linearization of the integral equations of ODT are discussed. The formalism for the slab measurement geometry is developed in Sec. III. Various particular cases are also consdidered, some of which have been implemented earlier, such as Fourier and paraxial tomography. In Sec. IV we suggest a novel multiprojection imaging modality and derive related inversion formulas. In Sec. V the cylindrical measurement geometry is considered. In Sec. VI we give examples of calculating the kernels for the integral equations considered in this paper. Finally, Sec. VII contains a summary of the results of this paper.

II. LINEAR INTEGRAL EQUATIONS

In this section we review several methods for linearization of integral equations for the operator V. The first Born and

first Rytov approximations are often used in ODT. In addition to these two methods we introduce a new approach based on an analogy with the mean-field approximation. For simplicity, we consider the $\hat{\mathbf{s}}$-independent Green's function for the DE, $G(\mathbf{r},\mathbf{r}')=\langle\mathbf{r}|G|\mathbf{r}'\rangle$ and use Eq. (19) to relate it to the measurable signal, but the same perturbative analysis applies to the Green's function $G(\mathbf{r},\hat{\mathbf{s}};\mathbf{r}',\hat{\mathbf{s}}')$.

In the coordinate representation, the first Born approximation (3) is of the form

$$G(\mathbf{r}_s,\mathbf{r}_d)=G_0(\mathbf{r}_s,\mathbf{r}_d)-\langle\mathbf{r}_s|G_0VG_0|\mathbf{r}_d\rangle, \tag{22}$$

where

$$\langle\mathbf{r}_s|G_0VG_0|\mathbf{r}_d\rangle=\int G_0(\mathbf{r}_s,\mathbf{r})V(\mathbf{r})G_0(\mathbf{r},\mathbf{r}_d)d^3r. \tag{23}$$

Consequently, the data function defined by

$$\phi(\mathbf{r}_s,\mathbf{r}_d)=\left(1+\frac{\ell^*}{\ell}\right)^2[G_0(\mathbf{r}_s,\mathbf{r}_d)-G(\mathbf{r}_s,\mathbf{r}_d)] \tag{24}$$

satisfies the linear integral equation

$$\phi(\mathbf{r}_s,\mathbf{r}_d)=\left(1+\frac{\ell^*}{\ell}\right)^2\int G_0(\mathbf{r}_s,\mathbf{r})V(\mathbf{r})G_0(\mathbf{r},\mathbf{r}_d)d^3r. \tag{25}$$

Here the factor $(1+\ell^*/\ell)^2$ is retained for the reasons discussed in Sec. I B and the constant $c\mu_s'\ell^*/4\pi$ omitted. Equation (24) is used to calculate ϕ from G, while in Eq. (25), ϕ must be regarded as given and V as unknown. Note that Eq. (25) has the same form as Eq. (4).

The first Rytov approximation is also frequently used. In this approximation G is given by

$$G(\mathbf{r}_s,\mathbf{r}_d)=G_0(\mathbf{r}_s,\mathbf{r}_d)\exp\left[-\frac{\langle\mathbf{r}_s|G_0VG_0|\mathbf{r}_d\rangle}{G_0(\mathbf{r}_s,\mathbf{r}_d)}\right]. \tag{26}$$

Equation (26) can be brought to the form (25) by using the following definition for the data function:

$$\phi(\mathbf{r}_s,\mathbf{r}_d)=-\left(1+\frac{\ell^*}{\ell}\right)^2G_0(\mathbf{r}_s,\mathbf{r}_d)\ln\left[\frac{G(\mathbf{r}_s,\mathbf{r}_d)}{G_0(\mathbf{r}_s,\mathbf{r}_d)}\right]. \tag{27}$$

Here the term inside the logarithm can be identified as the transmission coefficient.

Another possible approach which is proposed in this paper is analogous to the mean-field approximation as applied in Ref. [17]. The mean-field approximation is obtained from the Dyson equation (2) by fixing the position of source and making the ansatz $G(\mathbf{r},\mathbf{r}_d)=a(\mathbf{r}_s,\mathbf{r}_d)G_0(\mathbf{r},\mathbf{r}_d)$. Substituting this expression into Eq. (2) we can formally solve for $a(\mathbf{r}_s,\mathbf{r}_d)$ and obtain:

$$G(\mathbf{r}_s,\mathbf{r}_d)=G_0(\mathbf{r}_s,\mathbf{r}_d)\left[1+\frac{\langle\mathbf{r}_s|G_0VG_0|\mathbf{r}_d\rangle}{G_0(\mathbf{r}_s,\mathbf{r}_d)}\right]^{-1}. \tag{28}$$

Equation (28) can be brought to the form (25) by defining the data function according to

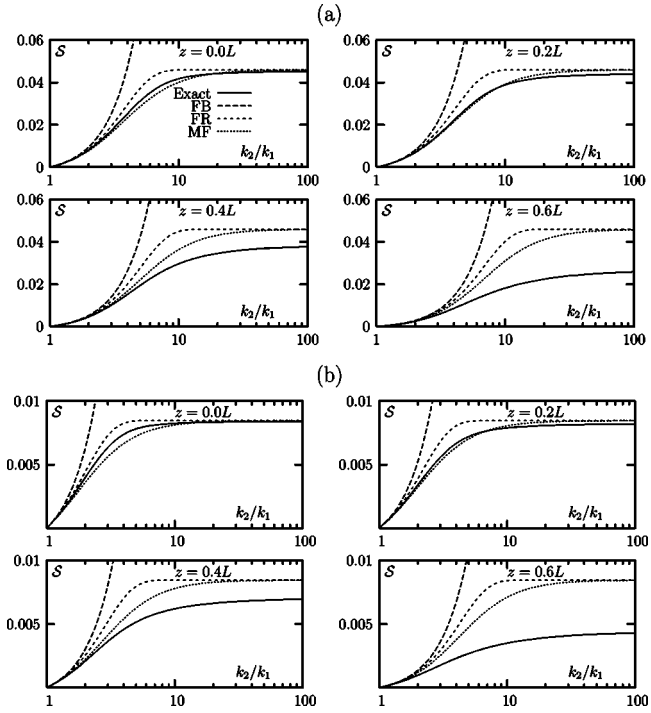

FIG. 1. The relative shadow $\mathcal{S}$ of a sphere of radius $R=0.4L$ with its center at the origin, as a function of k_2/k_1 for a source located at $(-L/2,0,z)$ and a detector located at $(L/2,0,z)$ and different values of z; $k_1L=1$ (a) and $k_1L=2$ (b).

$$\phi(\mathbf{r}_s,\mathbf{r}_d)=\left(1+\frac{\ell^*}{\ell}\right)^2\frac{G_0(\mathbf{r}_s,\mathbf{r}_d)}{G(\mathbf{r}_s,\mathbf{r}_d)}[G_0(\mathbf{r}_s,\mathbf{r}_d)-G(\mathbf{r}_s,\mathbf{r}_d)]. \tag{29}$$

The application of different forms of perturbation theory, as discussed above, to calculating the Green's function for the DE is illustrated in Fig. 1. We have considered a model situation of a spherical inhomogeneity of radius R characterized by the diffuse wave number $k_2=\sqrt{\alpha_2/D_2}$ embedded in an infinite medium with the diffuse wave number $k_1=\sqrt{\alpha_1/D_1}$, where $\alpha_{1,2}$ and $D_{1,2}$ are the absorption and diffusion coefficients in the background medium and inside the sphere, respectively. The Green's function can be found in this case analytically from the scalar wave Mie solution for imaginary wave numbers. Placing the origin at the center of the sphere, we obtain $G(\mathbf{r}_s,\mathbf{r}_d)=G_0(\mathbf{r}_s,\mathbf{r}_d)-(2k_1/\pi D_1)\mathcal{S}(\mathbf{r}_s,\mathbf{r}_d)$. Here the dimensionless relative shadow $\mathcal{S}(\mathbf{r}_s,\mathbf{r}_d)$ is given by

$$\mathcal{S}(\mathbf{r}_s,\mathbf{r}_d)=\sum_{l=0}^{\infty}\frac{(2l+1)a_l}{4\pi}P_l(\hat{\mathbf{r}}_s\cdot\hat{\mathbf{r}}_d), \tag{30}$$

with a_l being the Mie coefficients:

$$a_l=\frac{mi_l(k_1R)i_l'(k_2R)-i_l(k_2R)i_l'(k_1R)}{mi_l'(k_2R)k_l(k_1R)-i_l(k_2R)k_l'(k_1R)}, \tag{31}$$

where $m=k_2/k_1$, $P_l(x)$ are the Legendre polynomials, $i_l(x),k_l(x)$ are the modified spherical Bessel and Hankel functions of the first kind, the prime denotes differentiation of functions with respect to the argument in the parentheses,

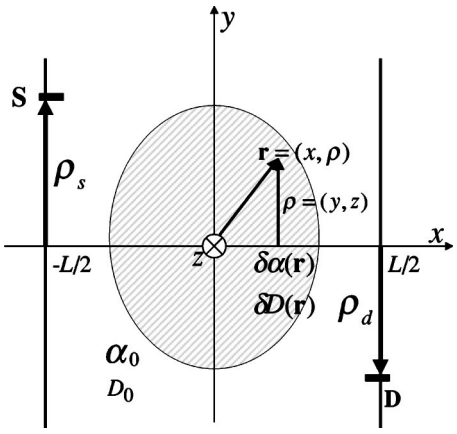

FIG. 2. Sketch of the experimental setup in the planar geometry (transmission measurements).

and the points $\mathbf{r}_s, \mathbf{r}_d$ are outside of the sphere ($r_s, r_d > R$).

In Fig. 1, $\mathcal{S}$ is plotted as a function of the ratio k_2/k_1 for different source detector pairs. The locations of the sources and detectors are specified in a Cartesian reference frame (x,y,z) with the origin in the center of the sphere by $\mathbf{r}_s = (-L/2, 0, z)$ and $\mathbf{r}_d = (L/2, 0, z)$ where z can take different values. The sphere radius was chosen to be $R = 0.4L$. It can be seen that, in most cases, the mean-field approximation is superior to the first Rytov, and the first Rytov is, in turn, superior to the Born. It should be kept in mind that to obtain the contrast of the absorption or diffusion coefficient, the value of k_2/k_1 must be squared. Thus a tenfold increase of the absorption coefficient inside the sphere corresponds to $k_2/k_1 \approx 3$.

III. PLANAR GEOMETRY

A. Integral equations in the planar geometry

The planar geometry is illustrated in Fig. 2. The medium to be imaged is located between two parallel measurement planes separated by the distance L. Intensity measurements are taken with multiple source-detector pairs denoted "S" and "D." We denote the coordinates of the sources and detectors as $\mathbf{r}_s = (x_s, \boldsymbol{\rho}_s)$ and $\mathbf{r}_d = (x_d, \boldsymbol{\rho}_d)$, respectively. Here $\boldsymbol{\rho}_{s,d} = (y_{s,d}, z_{s,d})$ are two-dimensional vectors parallel to the measurement planes. Without loss of generality, we assume that "transmission" measurements are performed with $x_s = -L/2$ and $x_d = L/2$, while "reflection" measurements with $x_s = x_d = -L/2$. A point inside the medium will be denoted $\mathbf{r} = (x, \boldsymbol{\rho})$, where $\boldsymbol{\rho} = (y,z)$ is a two-dimensional vector parallel to the measurement planes [18]. Further, it is assumed that the source and detector optical fibers are oriented perpendicular to the measurement surfaces and that their diameters are small compared to all other physically relevant scales. Therefore, the measured specific intensity is given, up to a multiplicative constant, by the Green's function $G(x_s, \boldsymbol{\rho}_s, \hat{\mathbf{s}}_s = \hat{\mathbf{x}}; x_d, \boldsymbol{\rho}_d, \hat{\mathbf{s}}_d = \pm\hat{\mathbf{x}})$, where plus corresponds to the transmission geometry and minus to the reflection geometry.

In each experiment, the parameters $x_s, x_d, \hat{\mathbf{s}}_s$, and $\hat{\mathbf{s}}_d$ are fixed. Therefore, we focus on the dependence of the data on $\boldsymbol{\rho}_s$, $\boldsymbol{\rho}_d$, and ω. Then, with use of one of the linearization methods discussed in Sec. II, we obtain the integral equation

$$\phi(\omega, \boldsymbol{\rho}_s, \boldsymbol{\rho}_d) = \int \Gamma(\omega, \boldsymbol{\rho}_s, \boldsymbol{\rho}_d; \mathbf{r})\, \eta(\mathbf{r}) d^3 r. \tag{32}$$

A few remarks concerning the above equation are necessary. First, the function ϕ is the experimentally measurable data function. To determine ϕ, it is necessary to know the full Green's function $G(x_s, \boldsymbol{\rho}_s, \hat{\mathbf{s}}_s; x_d, \boldsymbol{\rho}_d, \hat{\mathbf{s}}_d)$ as well as the unperturbed Green's function $G_0(x_s, \boldsymbol{\rho}_s, \hat{\mathbf{s}}_s; x_d, \boldsymbol{\rho}_d, \hat{\mathbf{s}}_d)$. The latter can be calculated analytically or, in some cases, measured experimentally using a homogeneous medium. The exact expression for ϕ in terms of G and G_0 depends on the linearization method used. Second, $\eta(\mathbf{r})$ is a vector representing the deviations of optical coefficients from their background values. Thus,

$$\eta(\mathbf{r}) = \begin{pmatrix} \delta\mu^*(\mathbf{r}) \\ \delta\mu_s'(\mathbf{r}) \end{pmatrix} (\text{for RTE}), \quad \eta(\mathbf{r}) = \begin{pmatrix} \delta\alpha(\mathbf{r}) \\ \delta D(\mathbf{r}) \end{pmatrix} (\text{for DE}). \tag{33}$$

Correspondingly, $\Gamma(\omega, \boldsymbol{\rho}_s, \boldsymbol{\rho}_d; \mathbf{r})$ is a vector of functions that multiply the respective coefficients. The specific form of Γ can be found if G_0 is known; we will give examples of such calculations in Sec. VI. Here we define

$$\Gamma(\omega, \boldsymbol{\rho}_s, \boldsymbol{\rho}_d; \mathbf{r}) = \begin{cases} (\Gamma_{\mu^*}(\omega, \boldsymbol{\rho}_s, \boldsymbol{\rho}_d; \mathbf{r}), \Gamma_{\mu_s'}(\omega, \boldsymbol{\rho}_s, \boldsymbol{\rho}_d; \mathbf{r})) & (\text{for RTE}), \\ (\Gamma_{\alpha}(\omega, \boldsymbol{\rho}_s, \boldsymbol{\rho}_d; \mathbf{r}), \Gamma_{D}(\omega, \boldsymbol{\rho}_s, \boldsymbol{\rho}_d; \mathbf{r})) & (\text{for DE}). \end{cases} \tag{34}$$

A fundamental property of the kernel Γ is its translational invariance. Mathematically, this means that $\Gamma(\omega, \boldsymbol{\rho}_s, \boldsymbol{\rho}_d; \mathbf{r})$ depends only on $\boldsymbol{\rho}_s - \boldsymbol{\rho}$ and $\boldsymbol{\rho}_d - \boldsymbol{\rho}$ rather than on the three parameters $\boldsymbol{\rho}_s$, $\boldsymbol{\rho}_d$, and $\boldsymbol{\rho}$ separately, so that the simultaneous transformation $\boldsymbol{\rho}_{s,d} \to \boldsymbol{\rho}_{s,d} + \mathbf{a}$, $\boldsymbol{\rho} \to \boldsymbol{\rho} + \mathbf{a}$ leaves the kernel invariant. Therefore, $\Gamma(\omega, \boldsymbol{\rho}_s, \boldsymbol{\rho}_d; \mathbf{r})$ can be written as the Fourier integral

$$\Gamma(\omega, \boldsymbol{\rho}_s, \boldsymbol{\rho}_d; \mathbf{r}) = \int \frac{d^2 q_s d^2 q_d}{(2\pi)^4} \kappa(\omega, \mathbf{q}_s, \mathbf{q}_d; x) \times \exp[i\mathbf{q}_s \cdot (\boldsymbol{\rho} - \boldsymbol{\rho}_s) + i\mathbf{q}_d \cdot (\boldsymbol{\rho}_d - \boldsymbol{\rho})], \tag{35}$$

where κ is the vector: $\kappa = (\kappa_{\mu^*}, \kappa_{\mu_s'})$ for the RTE and $\kappa = (\kappa_\alpha, \kappa_D)$ for the DE. Note that the isotropy of space requires that κ depend only on the absolute values of the two-dimensional vectors $\mathbf{q}_{s,d}$.

By introducing the new variables $\Delta\boldsymbol{\rho}$, $\mathbf{q}$, and $\mathbf{p}$ according to $\boldsymbol{\rho}_d = \boldsymbol{\rho}_s + \Delta\boldsymbol{\rho}$ and $\mathbf{q}_s = \mathbf{q} + \mathbf{p}$, $\mathbf{q}_d = \mathbf{p}$, we find that

$$\Gamma(\omega, \Delta\boldsymbol{\rho}, \boldsymbol{\rho}_s; \mathbf{r}) = \int \frac{d^2 q}{(2\pi)^2} K(\omega, \Delta\boldsymbol{\rho}, \mathbf{q}; x) \exp[i\mathbf{q} \cdot (\boldsymbol{\rho} - \boldsymbol{\rho}_s)], \tag{36}$$

where

$$K(\omega,\Delta\boldsymbol{\rho},\mathbf{q};x)=\int\frac{d^2p}{(2\pi)^2}\kappa(\omega,\mathbf{q}+\mathbf{p},\mathbf{p};x)\exp(i\mathbf{p}\cdot\Delta\boldsymbol{\rho}) \tag{37}$$

and the integral Eq. (32) takes the form

$$\phi(\omega,\Delta\boldsymbol{\rho},\boldsymbol{\rho}_s)=\int\Gamma(\omega,\Delta\boldsymbol{\rho},\boldsymbol{\rho}_s;\mathbf{r})\,\eta(\mathbf{r})d^3r. \tag{38}$$

Note that in Eqs. (36)–(38) the list of formal arguments of Γ and ϕ has been changed. Thus, for example, the data function $\phi(\omega,\boldsymbol{\rho}_s,\boldsymbol{\rho}_s+\Delta\boldsymbol{\rho})$ is replaced by $\phi(\omega,\Delta\boldsymbol{\rho},\boldsymbol{\rho}_s)$.

We now discuss the sampling of data. First, we assume that the sources are located on a square lattice with lattice spacing h so that $\boldsymbol{\rho}_s=h(\hat{\mathbf{y}}n_y+\hat{\mathbf{z}}n_z)$ where n_y and n_z are integers. Second, the vectors $\Delta\boldsymbol{\rho}$, which specify the source-detector transverse separation, are assumed to belong to the set Σ, $\Delta\boldsymbol{\rho}\in\Sigma$. In particular, Σ can be a square lattice, commensurate with the lattice of sources, with a spacing $h'\leqslant h$. Another case arises when the detectors continuously occupy the whole plane. Finally, the modulation frequencies belong to a finite set $\{\omega_j;j=1,2,\ldots,N_\omega\}$.

We also consider an approach in which N_d different linear combinations (with complex coefficients c_{ij}) of detector outputs are directly measured, allowing for the possibility of a phased-array measurement scheme. In this case, Eqs. (36) and (37) must be modified according to

$$\Gamma(\omega,i,\boldsymbol{\rho}_s;\mathbf{r})=\int\frac{d^2q}{(2\pi)^2}K(\omega,i,\mathbf{q};x)\exp[i\mathbf{q}\cdot(\boldsymbol{\rho}-\boldsymbol{\rho}_s)],$$

$$i=1,\ldots,N_d, \tag{39}$$

$$K(\omega,i,\mathbf{q};x)=\int\frac{d^2p}{(2\pi)^2}\kappa(\omega,\mathbf{q}+\mathbf{p},\mathbf{p};x)\sum_{\Delta\boldsymbol{\rho}_j\in\Sigma}c_{ij}\exp(i\mathbf{p}\cdot\Delta\boldsymbol{\rho}_j),$$

$$i=1,\ldots,N_d, \tag{40}$$

and the integral equation for phased-array measurements becomes

$$\phi(\omega,i,\boldsymbol{\rho}_s)=\int\Gamma(\omega,i,\boldsymbol{\rho}_s;\mathbf{r})\,\eta(\mathbf{r})d^3r,\quad i=1,\ldots,N_d, \tag{41}$$

where

$$\phi(\omega,i,\boldsymbol{\rho}_s)=\sum_{\Delta\boldsymbol{\rho}_j\in\Sigma}c_{ij}\phi(\omega,\Delta\boldsymbol{\rho}_j,\boldsymbol{\rho}_s),\quad i=1,\ldots,N_d. \tag{42}$$

Note that the matrix c_{ij} does not need to be square; in the case of a continuous set Σ, the summation must be replaced by integration and c_{ij} by a vector of functions $c_i(\Delta\boldsymbol{\rho})$.

B. Inversion formulas

It is convenient to define a new three-dimensional variable $\mu=(\omega,\Delta\boldsymbol{\rho})$ or $\mu=(\omega,i)$, with Λ the set of such μ, and rewrite Eq. (42) as

$$\phi(\mu,\boldsymbol{\rho}_s)=\int\Gamma(\mu,\boldsymbol{\rho}_s;\mathbf{r})\,\eta(\mathbf{r})d^3r. \tag{43}$$

The integral operator Γ defines a map between two different Hilbert spaces $\mathcal{H}_1$ and $\mathcal{H}_2$. Equation (43) can be written in Dirac notation as

$$|\phi\rangle=\Gamma|\eta\rangle. \tag{44}$$

The pseudoinverse solution to Eq. (44) is given by

$$|\eta\rangle=\Gamma^+|\phi\rangle. \tag{45}$$

Here the pseudoinverse operator Γ^+ is given by

$$\Gamma^+=(\Gamma^*\Gamma)^{-1}\Gamma^*=\Gamma^*(\Gamma\Gamma^*)^{-1}, \tag{46}$$

where " $*$" denotes Hermitian conjugation and the expressions $(\Gamma^*\Gamma)^{-1}$ and $(\Gamma\Gamma^*)^{-1}$ must be appropriately regularized. The regularized singular-value decomposition (SVD) of the pseudoinverse operator is given by

$$\Gamma^+=\sum_n\Theta(\sigma_n,\epsilon)\frac{|g_n\rangle\langle f_n|}{\sigma_n}, \tag{47}$$

where $\Theta(x,\epsilon)$ is an appropriate regularizer, ϵ is a small regularization parameter, and the singular functions $|f_n\rangle$ and $|g_n\rangle$ are eigenfunctions with eigenvalues σ_n^2 of the operators $\Gamma\Gamma^*$ and $\Gamma^*\Gamma$, respectively:

$$\Gamma\Gamma^*|f_n\rangle=\sigma_n^2|f_n\rangle,\quad \Gamma^*\Gamma|g_n\rangle=\sigma_n^2|g_n\rangle. \tag{48}$$

In addition, the following relations hold:

$$\Gamma^*|f_n\rangle=\sigma_n|g_n\rangle,\quad \Gamma|g_n\rangle=\sigma|f_n\rangle. \tag{49}$$

To obtain the SVD for the pseudoinverse operator, we first consider the eigenfunctions and eigenvalues of the operator $\Gamma\Gamma^*$. Its matrix elements in the basis $|\mu\boldsymbol{\rho}_s\rangle$ are given by

$$\langle\mu\boldsymbol{\rho}_s|\Gamma\Gamma^*|\mu'\boldsymbol{\rho}_s'\rangle=\int\frac{d^2q}{(2\pi)^2}\langle\mu|M_1(\mathbf{q})|\mu'\rangle\times\exp[-i\mathbf{q}\cdot(\boldsymbol{\rho}_s-\boldsymbol{\rho}_s')], \tag{50}$$

where

$$\langle\mu|M_1(\mathbf{q})|\mu'\rangle=\int_{-L/2}^{L/2}K(\mu,\mathbf{q};x)K^*(\mu',\mathbf{q};x)dx. \tag{51}$$

From Eq. (50), it can be seen that the effective dimensionality of the eigenproblem can be reduced. That is, the $\boldsymbol{\rho}_s$-dependent part of the eigenfunctions can be found analytically. Indeed, the ansatz

$$\langle\mu\rho_s|f_{\nu\mathbf{u}}\rangle=\frac{h}{2\pi}\exp(-i\mathbf{u}\cdot\boldsymbol{\rho}_s)\langle\mu|C_\nu(\mathbf{u})\rangle, \tag{52}$$

where ν and $\mathbf{u}$ are the indexes that label the eigenfunctions with $\mu,\nu\in\Lambda$ and $\mathbf{u}$ is a two-dimensional vector in the first Brillouin zone (FBZ) of the lattice on which the sources are placed, $-\pi/h\leqslant u_y,u_z\leqslant\pi/h$. It can be verified that $|f_{\nu\mathbf{u}}\rangle$ are eigenfunctions of $\Gamma\Gamma^*$ if $|C_\nu(\mathbf{u})\rangle$ are eigenvectors of the matrix $M(\mathbf{u})$ defined by

$$M(\mathbf{u}) = \sum_{\mathbf{v}} M_1(\mathbf{u}+\mathbf{v}), \tag{53}$$

where the $\mathbf{v}$'s are reciprocal lattice vectors, $\mathbf{v}=(2\pi/h)(n_y\hat{\mathbf{y}}+n_z\hat{\mathbf{z}})$. We denote the eigenvalues of the non-negative definite matrix $M(\mathbf{u})$ by $M_\nu^2(\mathbf{u})$ and the singular values of the problem (the eigenvalues of $\Gamma\Gamma^*$) by $\sigma_{\nu\mathbf{u}}^2$. Then the following relations hold:

$$M(\mathbf{u})|C_\nu(\mathbf{u})\rangle = M_\nu^2(\mathbf{u})|C_\nu(\mathbf{u})\rangle, \tag{54}$$

$$\Gamma\Gamma^*|f_{\nu\mathbf{u}}\rangle = \sigma_{\nu\mathbf{u}}^2|f_{\nu\mathbf{u}}\rangle, \tag{55}$$

$$\sigma_{\nu\mathbf{u}} = h^{-1}M_\nu(\mathbf{u}). \tag{56}$$

Note that the singular functions $|f_{\nu\mathbf{u}}\rangle$, Eq. (52), are normalized according to $\langle f_{\nu\mathbf{u}}|f_{\nu'\mathbf{u}'}\rangle=\delta_{\nu\nu'}\delta(\mathbf{u}-\mathbf{u}')$.

The second set of singular functions, $|g_{\nu\mathbf{u}}\rangle$, can be obtained from the relations (49):

$$\langle x\boldsymbol{\rho}|g_{\nu\mathbf{u}}\rangle = \frac{1}{2\pi h\sigma_{\nu\mathbf{u}}}\exp(-i\mathbf{u}\cdot\boldsymbol{\rho})\sum_{\mu} P^*(\mu,\mathbf{u};x,\boldsymbol{\rho})\langle\mu|C_\nu(\mathbf{u})\rangle, \tag{57}$$

where

$$P(\mu,\mathbf{u};x,\boldsymbol{\rho}) = \sum_{\mathbf{v}} K(\mu,\mathbf{u}+\mathbf{v};x)\exp(i\mathbf{v}\cdot\boldsymbol{\rho}). \tag{58}$$

To obtain an inversion formula, according to Eq. (45) and (47), we need to evaluate the scalar product $\langle f_{\nu\mathbf{u}}|\phi\rangle$. It can be shown by direct calculation that

$$\langle f_{\nu\mathbf{u}}|\phi\rangle = \frac{h}{2\pi}\sum_{\mu}\langle C_\nu(\mathbf{u})|\mu\rangle\tilde{\phi}(\mu,\mathbf{u}), \tag{59}$$

where $\tilde{\phi}(\mu,\mathbf{u})$ is the lattice Fourier transform of $\phi(\mu,\boldsymbol{\rho}_s)$ with respect to $\boldsymbol{\rho}_s$:

$$\tilde{\phi}(\mu,\mathbf{u}) = \sum_{\boldsymbol{\rho}_s}\phi(\mu,\boldsymbol{\rho}_s)\exp(i\mathbf{u}\cdot\boldsymbol{\rho}_s). \tag{60}$$

Finally, we arrive at the following inversion formula:

$$\eta(\mathbf{r}) = \sum_\nu \int_{\mathrm{FBZ}} \frac{d^2u}{(2\pi)^2}\frac{1}{\sigma_{\nu\mathbf{u}}^2}\Theta(\sigma_{\nu\mathbf{u}},\epsilon)\exp(-i\mathbf{u}\cdot\boldsymbol{\rho}) \times\sum_{\mu,\mu'} P^*(\mu,\mathbf{u};\mathbf{r})\langle\mu|C_\nu(\mathbf{u})\rangle\langle C_\nu(\mathbf{u})|\mu'\rangle\tilde{\phi}(\mu',\mathbf{u}). \tag{61}$$

The above result can be simplified by noting the relation

$$\sum_\nu \Theta(\sigma_{\nu\mathbf{u}},\epsilon)\frac{|C_\nu(\mathbf{u})\rangle\langle C_\nu(\mathbf{u})|}{M_{\nu\mathbf{u}}^2} = M^{-1}(\mathbf{u}). \tag{62}$$

Using the above relation, the inversion formula (61) can be rewritten as

$$\eta(\mathbf{r}) = h^2\int_{\mathrm{FBZ}}\frac{d^2u}{(2\pi)^2}\exp(-i\mathbf{u}\cdot\boldsymbol{\rho})\sum_{\mu,\mu'} P^*(\mu,\mathbf{u};\mathbf{r}) \times\langle\mu|M^{-1}(\mathbf{u})|\mu'\rangle\tilde{\phi}(\mu',\mathbf{u}), \tag{63}$$

which is our main result pertaining to the planar geometry.

Several comments on the above result are necessary.

(i) The pseudoinverse solution (63) was derived under the assumption that the sources occupy an infinite lattice. In practice, however, they must be restricted to a finite spatial window. In this case, the inversion formula (63) is no longer exact. However, if the edges of the window are sufficiently far from the inhomogeneities of the medium, a good approximation to the pseudoinverse solution may be obtained. This is due to the exponential decay of the Green's functions in an absorbing medium (for both the RTE and DE).

(ii) The variable $\mathbf{u}$ is continuous, but, in practice, must be discretized. The number of discrete vectors $\mathbf{u}$ should roughly correspond to the number of different sources used in the experiment. As discussed above, this is a finite number which we denote by N_1. We will refer to N_1 as the number of *external* degrees of freedom. Next, let the variable μ run over N_2 discrete points. Here N_2 is the number of the "internal" degrees of freedom. A purely numerical SVD inversion requires diagonalizing a matrix of size N_1N_2 which has computational complexity $O((N_1N_2)^3)$. However, the inversion formula (63) requires only N_1 diagonalizations of the matrix $M(\mathbf{u})$ whose size is N_2 (hence the terms "external" and "internal" degrees of freedom). The computational complexity of this procedure is $O(N_1N_2^3)$, which is N_1^2 times smaller than that for the purely numerical method. For large N_1, this is an enormous advantage. Note that one should add to the above estimate the number of operations necessary to Fourier-transform the data function and to sum over the variables μ,μ' and $\mathbf{u}$ in Eq. (63). The computational cost of the first task scales as $O(N_1\log N_1)$ with the use of the fast Fourier transform and, if $\log N_1 \ll N_2^3$, can be neglected. The second task requires $O(N_1N_2^2)$ operations, which is also negligible.

(iii) It can be seen from the inversion formula (63) that the transverse resolution of the reconstruction is at most the lattice step h. Therefore, it is necessary to evaluate the function $\eta(\mathbf{r})=\eta(x,\boldsymbol{\rho})$ only at those points $\boldsymbol{\rho}$ which lie in the source lattice. In this case, the factor $\exp(i\mathbf{v}\cdot\boldsymbol{\rho})$ in the definition of $P(\mu,\mathbf{u};x,\boldsymbol{\rho})$, Eq. (58), is equal to unity. Consequently, P becomes independent of $\boldsymbol{\rho}$ and is denoted $P(\mu,\mathbf{u};x)$. Then the double sum in Eq. (63) is a function of $\mathbf{u}$ and x only. This fact significantly improves the computational performance of the algorithm.

(iv) So far we have placed no restrictions on $\eta(x,\boldsymbol{\rho})$ except for square integrability. In some cases it is known *a priori* that $\eta(x,\boldsymbol{\rho})$ is smooth. In particular, consider the case when it is known that the Fourier transform $\hat{\eta}(x,\mathbf{q})$ of the function η vanishes if $|q_y|>\pi/h$ or $|q_z|>\pi/h$:

$$\hat{\eta}(x,\mathbf{q}) = \int \eta(x,\boldsymbol{\rho})\exp(i\mathbf{q}\cdot\boldsymbol{\rho})d^2\rho = 0, \quad \text{if } \mathbf{q}\notin \mathrm{FBZ}. \tag{64}$$

Functions which satisfy Eq. (64) are said to be transversely band limited to the FBZ of the source lattice. The operator Γ

maps the Hilbert space of such functions, H_1^{b}, to the Hilbert space of the data, H_2, and can be written as

$$\Gamma(\mu,\boldsymbol{\rho}_s;\mathbf{r}) = \int_{\mathrm{FBZ}} \frac{d^2u}{(2\pi)^2} K(\mu,\mathbf{q};x)\exp[i\mathbf{u}\cdot(\boldsymbol{\rho}-\boldsymbol{\rho}_s)]. \tag{65}$$

Note that integration in Eq. (65) over d^2u is limited to the FBZ, in contrast to the analogous equation (36) where integration over d^2q is carried out over the entire Fourier space. However, the two operators (65) and (36) are equivalent if they act on the space H_1^{b}. This fact can be used to show that the SVD pseudoinverse solution on the space of transversely band-limited functions η has the form

$$\eta(\mathbf{r}) = h^2 \int_{\mathrm{FBZ}} \frac{d^2u}{(2\pi)^2} \exp(-i\mathbf{u}\cdot\boldsymbol{\rho}) \sum_{\mu,\mu'} K^*(\mu,\mathbf{u};x) \times \langle\mu|M_1^{-1}(\mathbf{u})|\mu'\rangle \tilde{\phi}(\mu',\mathbf{u}), \tag{66}$$

where M_1 is given by Eq. (51). Thus, the summation over the reciprocal lattice vectors that is required for the calculation of P and M in the inversion formula (63) is avoided if it is known that η is transversely band limited.

(v) Consider the limit $h\to 0$, which corresponds to the case of continuous data. In this case the reciprocal lattice vectors become infinite, except for $\mathbf{v}=0$. Since the functions $K(\mu,\mathbf{q};x)$ decay exponentially with $|\mathbf{q}|$, we have in this limit $M(\mathbf{u})=M_1(\mathbf{u})$ and $P(\mu,\mathbf{u};x,\boldsymbol{\rho})=K(\mu,\mathbf{u};x)$. We also use the relation $\lim_{h\to 0}(h^2\tilde{\phi})=\hat{\phi}$, where $\hat{\phi}$ is the continuous Fourier transform of the data function defined by

$$\hat{\phi}(\mu,\mathbf{u}) = \int d^2\rho_s \phi(\mu,\boldsymbol{\rho}_s)\exp(i\mathbf{u}\cdot\boldsymbol{\rho}_s), \tag{67}$$

to show that, in the limit $h\to 0$, the inversion formula (63) becomes

$$\eta(\mathbf{r}) = \int \frac{d^2q}{(2\pi)^2} \exp(-i\mathbf{q}\cdot\boldsymbol{\rho}) \sum_{\mu,\mu'} K^*(\mu,\mathbf{q};x) \times \langle\mu|M_1^{-1}(\mathbf{q})|\mu'\rangle \hat{\phi}(\mu',\mathbf{q}). \tag{68}$$

This reconstruction formula was implemented in [10,11,14].

C. Special cases

1. Fourier tomography

In this section we consider the case when the source and detector lattices are commensurate and, further, that the lattice of sources is a sublattice of the lattice of detectors. More specifically, let $\boldsymbol{\rho}_s=h_s(\hat{\mathbf{y}}n_{sy}+\hat{\mathbf{z}}n_{sz})$ and $\boldsymbol{\rho}_d=h_d(\hat{\mathbf{y}}n_{dy}+\hat{\mathbf{z}}n_{dz})$ where n_{sy}, n_{sz}, n_{dy}, n_{dz}, and h_s/h_d is an integer ($h_s \geqslant h_d$). We will show that the reconstruction formulas in the case considered here contain a double Fourier transform of the data function $\phi(\omega,\boldsymbol{\rho}_s,\boldsymbol{\rho}_d)$ with respect to the variables $\boldsymbol{\rho}_s$ and $\boldsymbol{\rho}_d$.

First, consider the expression (37) for $K(\omega,\Delta\boldsymbol{\rho},\mathbf{q};x)$. For commensurate lattices and $h_d \leqslant h_s$, it can be seen that $\Delta\boldsymbol{\rho}$ lies in the same lattice as $\boldsymbol{\rho}_d$. Therefore, Eq. (37) can be rewritten as

$$K(\omega,\Delta\boldsymbol{\rho},\mathbf{q};x) = \int_{\mathrm{FBZ}(h_d)} \frac{d^2w}{(2\pi)^2} \sum_{\mathbf{v}_d} \kappa(\omega,\mathbf{q}+\mathbf{w}+\mathbf{v}_d, \mathbf{w}+\mathbf{v}_d;x)\exp(i\mathbf{w}\cdot\Delta\boldsymbol{\rho}). \tag{69}$$

Here integration is carried out over the first Brillouin zone of the lattice with spacing h_d [FBZ(h_d)] and $\mathbf{v}_d=(2\pi/h_d)(\hat{\mathbf{y}}n_y+\hat{\mathbf{z}}n_z)$ is a reciprocal lattice vector of the same lattice. Substituting Eq. (69) into Eqs. (51) and (53), we obtain the following expression for the elements of the matrix $M(\mathbf{u})$:

$$\langle\mu|M(\mathbf{u})|\mu'\rangle = \int_{\mathrm{FBZ}(h_d)} \frac{d^2w d^2w'}{(2\pi)^4} \langle\omega\mathbf{w}|\tilde{M}(\mathbf{u})|\omega'\mathbf{w}'\rangle \times \exp[i(\mathbf{w}\cdot\Delta\boldsymbol{\rho}-\mathbf{w}'\cdot\Delta\boldsymbol{\rho}')], \tag{70}$$

where

$$\langle\omega\mathbf{w}|\tilde{M}(\mathbf{u})|\omega'\mathbf{w}'\rangle = \sum_{\mathbf{v}_s} \sum_{\mathbf{v}_d,\mathbf{v}_d'} \langle\omega,\mathbf{w}+\mathbf{v}_d|\tilde{M}_1(\mathbf{u}+\mathbf{v}_s)|\omega',\mathbf{w}'+\mathbf{v}_d'\rangle \tag{71}$$

and

$$\langle\omega\mathbf{p}|\tilde{M}_1(\mathbf{q})|\omega'\mathbf{p}'\rangle = \int_{-L/2}^{L/2} \kappa(\omega,\mathbf{q}+\mathbf{p},\mathbf{p};x) \times \kappa^*(\omega',\mathbf{q}+\mathbf{p}',\mathbf{p}';x)dx. \tag{72}$$

Here $\mathbf{v}_s$ is a reciprocal lattice vector for the lattice with spacing h_s, $\mathbf{u}$ lies in the FBZ(h_s), and $\langle\omega\mathbf{w}|\tilde{M}(\mathbf{u})|\omega'\mathbf{w}'\rangle$ can be viewed as the Fourier transform of $\langle\omega\Delta\boldsymbol{\rho}|M(\mathbf{u})|\omega'\Delta\boldsymbol{\rho}'\rangle$ with respect to the variables $\Delta\boldsymbol{\rho}$ and $\Delta\boldsymbol{\rho}'$.

It can be easily verified that the inverse of the matrix $M(\mathbf{u})$ is given in terms of the inverse of $\tilde{M}(\mathbf{u})$ by the following formula:

$$\langle\mu|M^{-1}(\mathbf{u})|\mu'\rangle = h_d^4 \int_{\mathrm{FBZ}(h_d)} d^2w d^2w' \langle\omega\mathbf{w}|\tilde{M}^{-1}(\mathbf{u})|\omega'\mathbf{w}'\rangle \times \exp[i(\mathbf{w}\cdot\Delta\boldsymbol{\rho}-\mathbf{w}'\cdot\Delta\boldsymbol{\rho}')]. \tag{73}$$

Next we substitute Eq. (73) into the inversion formula (63) and obtain the following result:

$$\eta(\mathbf{r}) = (h_s h_d)^2 \int_{\mathrm{FBZ}(h_s)} \frac{d^2u}{(2\pi)^2} \exp(-i\mathbf{u}\cdot\boldsymbol{\rho}) \times \sum_{\omega,\omega'} \int_{\mathrm{FBZ}(h_d)} d^2w \int_{\mathrm{FBZ}(h_d)} d^2w' \tilde{P}^*(\omega,\mathbf{w},\mathbf{u};\mathbf{r}) \times \langle\omega\mathbf{w}|\tilde{M}^{-1}(\mathbf{u})|\omega'\mathbf{w}'\rangle \tilde{\phi}(\omega',\mathbf{u}+\mathbf{w}',-\mathbf{w}'), \tag{74}$$

where

$$\tilde{P}(\omega,\mathbf{w},\mathbf{u};\mathbf{r}) = \sum_{\mathbf{v}_s,\mathbf{v}_d} \kappa(\omega,\mathbf{u}+\mathbf{v}_s+\mathbf{w}+\mathbf{v}_d,\mathbf{w}+\mathbf{v}_d;x)\exp(i\mathbf{v}_s\cdot\boldsymbol{\rho}) \tag{75}$$

and

$$\tilde{\phi}(\omega,\mathbf{q}_s,\mathbf{q}_d)=\sum_{\boldsymbol{\rho}_s,\boldsymbol{\rho}_d}\phi(\omega,\boldsymbol{\rho}_s,\boldsymbol{\rho}_d)\exp[i(\mathbf{q}_s\cdot\boldsymbol{\rho}_s+\mathbf{q}_d\cdot\boldsymbol{\rho}_d)]. \tag{76}$$

Note that here we use the original notation $\phi=\phi(\omega,\boldsymbol{\rho}_s,\boldsymbol{\rho}_d)$ where $\boldsymbol{\rho}_s$ and $\boldsymbol{\rho}_d$ are the coordinates of the source and detector, respectively.

An important feature of this inversion formula is that it avoids numerical evaluation of the two-dimensional integral (37) which must be performed for every value of $\Delta\boldsymbol{\rho}$, $\mathbf{q}$, and x used in the inversion formulas. Note that the functions $\tilde{P}(\omega,\mathbf{w},\mathbf{u};\mathbf{r})$ and $\tilde{M}(\mathbf{u})$ appearing in the inversion formula (74) are expressed directly in terms of the functions κ. The price of this simplification is that the operator $\tilde{M}$ is continuous (unlike the matrix M). This problem is, however, easily avoided by replacing the integral over d^2wd^2w' by a double sum over a finite set of discrete vectors $\mathbf{w}_l$, $l=1,\ldots,N_w$:

$$\begin{aligned}\eta(\mathbf{r})=(h_sh_d)^2\int_{\mathrm{FBZ}(h_s)}\frac{d^2u}{(2\pi)^2}\exp(-i\mathbf{u}\cdot\boldsymbol{\rho})\\ \times\sum_{\omega,\omega'}\sum_{\mathbf{w},\mathbf{w}'}\tilde{P}^*(\omega,\mathbf{w},\mathbf{u};\mathbf{r})\langle\omega\mathbf{w}|\tilde{M}^{-1}(\mathbf{u})|\omega'\mathbf{w}'\rangle\\ \times\tilde{\phi}(\omega',\mathbf{u}+\mathbf{w}',-\mathbf{w}'),\end{aligned} \tag{77}$$

The discrete vectors $\mathbf{w}_l$ can be referred to as the "internal" degrees of freedom, similar to $\Delta\boldsymbol{\rho}$. The number and choice of $\mathbf{w}$'s used in the reconstruction algorithm will influence the depth resolution.

It is important to note that the expression (77) is no longer an SVD pseudoinverse solution with respect to all the available data $\phi(\omega,\boldsymbol{\rho}_s,\boldsymbol{\rho}_d)$. Instead, it can be shown that Eq. (77) gives the pseudoinverse solution of the Fourier-transformed data $\tilde{\phi}(\omega,\mathbf{u}+\mathbf{w},-\mathbf{w})$ where $\mathbf{u}\in\mathrm{FBZ}(h_s)$ is continuous while $\mathbf{w}\in\mathrm{FBZ}(h_d)$ is discrete.

The drawback of the Fourier method is that in order to obtain $\tilde{\phi}(\omega,\mathbf{u}+\mathbf{w},-\mathbf{w})$, the data function $\phi(\omega,\boldsymbol{\rho}_s,\boldsymbol{\rho}_d)$ must be experimentally measured for all possible points $\boldsymbol{\rho}_s,\boldsymbol{\rho}_d$, even if the number of discrete vectors $\mathbf{w}$ is small. It can be argued therefore that not all of the experimentally collected data are well used by this method.

In general, the number of modulation frequencies used in the Fourier method is arbitrary. However, two modulation frequencies (one of which can be zero) are sufficient to simultaneously reconstruct both absorbing and scattering inhomogeneities [10,14]. If one can assume that only absorbing inhomogeneities are present in the medium, a single modulation frequency is sufficient.

The region of the outermost integration in formulas (74) and (77) over d^2u is $\mathrm{FBZ}(h_s)$. It can be formally concluded that the transverse resolution in the reconstructed images is determined by the step of the coarser lattice (in this case, h_s). However, the dependence of the functions P on $\boldsymbol{\rho}$ through the exponential factors $\exp(i\mathbf{v}_s\cdot\boldsymbol{\rho})$ in conjunction with summation over discrete vectors $\mathbf{v}_s$ provides a possibility for superresolution. In the limiting case $h_s\to\infty$ when, essentially, only one source is used, the transverse resolution should remain finite. However, multiple modulation frequencies ω must be employed in this case to provide an additional degree of freedom and make the inverse problem well determined. In general, one can expect the transverse resolution to be somewhere in the interval $[h_d,h_s]$.

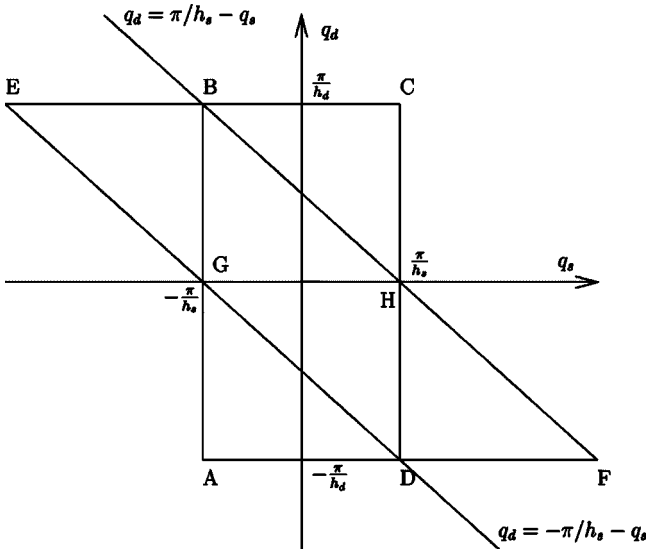

FIG. 3. Illustration of integration regions in reconstruction formula (74) with and without the blocking functions for the case $h_s=2h_d$. Only z components of vectors $\mathbf{q}_s=\mathbf{u}+\mathbf{w}'$ and $\mathbf{q}_d=-\mathbf{w}'$ are shown.

Finally, we discuss the use of blocking functions in the numerical implementation of reconstruction formulas (74) and (77). The blocking functions were introduced in [12,19] to avoid the use of redundant data. Indeed, the Fourier-transformed data function $\tilde{\phi}$ is periodic: $\tilde{\phi}(\omega,\mathbf{q}_s,\mathbf{q}_d)=\tilde{\phi}(\omega,\mathbf{q}_s+\mathbf{v}_s,\mathbf{q}_d+\mathbf{v}_d)$ where $\mathbf{v}_s$ and $\mathbf{v}_d$ is any of the discrete reciprocal lattice vectors defined above. Thus, if data are taken in more than one Brillouin zone, there is a chance that redundant (equivalent) data points will be used, which would provide no additional information. It can be easily seen by examining the limits of integration over d^2u and d^2w' that the argument $\mathbf{q}_s=\mathbf{u}+\mathbf{w}'$ of the data function can be in both the first and the second Brillouin zones of the reciprocal lattice of sources, even in the case $h_s=h_d$. In order to force this variable to stay in the $\mathrm{FBZ}(h_s)$, blocking functions were introduced with the following properties: $\chi(\mathbf{q}_s,\mathbf{q}_d)=1$ is $\mathbf{q}_s\in\mathrm{FBZ}(h_s)$ and $\mathbf{q}_d\in\mathrm{FBZ}(h_d)$, and $\chi(\mathbf{q}_s,\mathbf{q}_d)=0$ otherwise. In numerical implementations, the data function $\tilde{\phi}(\omega,\mathbf{q}_s,\mathbf{q}_d)$ is replaced by the product $\chi(\omega,\mathbf{q}_s,\mathbf{q}_d)\tilde{\phi}(\omega,\mathbf{q}_s,\mathbf{q}_d)$. The inversion formula (77) remains the pseudoinverse solution of the Fourier-transformed data as discussed above. However, we show below that the use of blocking functions is unnecessary and no redundant data are used in any of the inversion formulas discussed above. In fact, application of the blocking function method results in the use of only half of all available data points.

The region of integration in the inversion formulas (74) and (77) is illustrated in Fig. 3, where we have made the variable transformation $\mathbf{q}_s=\mathbf{u}+\mathbf{w}'$, $\mathbf{q}_d=-\mathbf{w}'$. We note that $-\pi/h_s\leqslant u_{y,z}<\pi/h_s$ and $-\pi/h_d\leqslant w'_{y,z}<\pi/h_d$. Thus, the area of integration in Eq. (74) is the figure *BHFDGE* while the

first Brillouin zone is *ABCD* (only z components of vectors are shown for the specific case $h_s=2h_d$). The use of blocking functions results in limiting the integration region to *BHDG* which is completely within the first Brillouin zone. Note that the area of *BHDG* is half that of *ABCD*, so that half of all available data points are discarded due to the use of blocking functions. But because of the periodicity of $\tilde{\phi}$ mentioned above, the data in the triangle *ABG* are equivalent to the data in the triangle *BCH*, which does not have any common internal points with *BHDG*. Analogously, the data in *DHF* are equivalent to the data in *ADG*. Thus, integration over the figure *BHFDGE* is equivalent to integration over *ABCD*. Therefore, the inversion formulas (74) and (77) do not utilize any redundant data.

A reconstruction algorithm based on the inversion formula (77) was implemented in [12]. In the limit h_s, $h_d\to 0$, this inversion formula takes the form

$$\eta(\mathbf{r}) = \int \frac{d^2q}{(2\pi)^2}\exp(-i\mathbf{q}\cdot\boldsymbol{\rho})\sum_{\omega,\omega'}\sum_{\mathbf{p},\mathbf{p}'}\kappa^*(\omega,\mathbf{q}+\mathbf{p},\mathbf{p};x) \times\langle\omega\mathbf{p}|\tilde{M}_1^{-1}(\mathbf{q})|\omega'\mathbf{p}'\rangle\hat{\phi}(\omega',\mathbf{q}+\mathbf{p}',-\mathbf{p}'), \qquad (78)$$

where $\hat{\phi}(\omega,\mathbf{q}_s,\mathbf{q}_d)$ is the continuous Fourier transform of $\phi(\omega,\boldsymbol{\rho}_s,\boldsymbol{\rho}_d)$ with respect to $\boldsymbol{\rho}_s$ and $\boldsymbol{\rho}_d$. The continuous version of the Fourier reconstruction algorithm was implemented in [10,11].

2. Real-space tomography

This imaging modality is based on direct application of the inversion formula (63), where the set Σ is assumed to contain enough points to make the inverse problem at least well determined. The main advantage of this method is that it uses real-space measurements as the input data and thus utilizes *all* experimental measurements in the most efficient way. However, numerical evaluation of the functions $K(\omega,\Delta\boldsymbol{\rho},\mathbf{q};x)$ according to the definition (37) is complicated, especially for large values of $|\Delta\boldsymbol{\rho}|$ when the integral is highly oscillatory.

3. Coaxial and paraxial tomography

The coaxial and paraxial measurement schemes are variants of the real-space method with the requirement that the number of discrete vectors $\Delta\boldsymbol{\rho}$ which are used be small and the source-detector transverse displacements satisfy $|\Delta\boldsymbol{\rho}| \ll L$. This inequality makes the numerical evaluation of the oscillatory integral (37) much easier. The additional degrees of freedom which are necessary to make the inverse problem well defined are obtained by considering many different modulation frequencies. Note that coaxial and paraxial tomography can be used only in the "transmission" geometry, when sources and detectors are placed on different planes.

In the coaxial measurement geometry only one value of $\Delta\boldsymbol{\rho}$ is used—namely, $\Delta\boldsymbol{\rho}=0$. Thus, the source and detector are always on axis. If only absorbing inhomogeneities are present, it can be seen by counting the degrees of freedom (two for source location plus one for modulation frequency) that the inverse problem is well determined in this case.

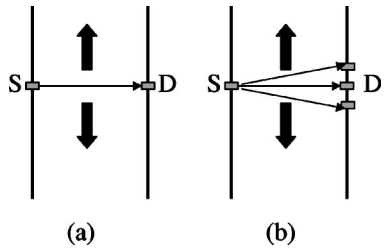

FIG. 4. Measurements scheme in the coaxial (a) and paraxial (b) cases.

However, there is a symmetry in the integral equations which would result in the appearance of "twinning" artifacts in the reconstructed images. Namely, the function $K(\omega,0,\mathbf{q};x)$ defined by Eq. (37) is symmetric in x: $K(\omega,0,\mathbf{q};x)=K(\omega,0,\mathbf{q};-x)$. Therefore, an inhomogeneity $\eta(x,\boldsymbol{\rho})$ and its mirror image with respect to the plane $x=0$, $\eta'(x,\boldsymbol{\rho})=\eta(-x,\boldsymbol{\rho})$ would result in the same data function ϕ. In this situation, the SVD pseudoinverse solution would yield (assuming infinite numerical precision of computations and an infinite set of modulation frequencies) the function $\eta''=(\eta+\eta')/2$. Thus, if a medium has an inhomogeneity at the point (x_0,y_0,z_0), the pseudoinverse solution would show an inhomogeneity at this point and at its mirror image $(-x_0,y_0,z_0)$. The problem is solved by using paraxial data (with $0<|\Delta\boldsymbol{\rho}|\ll L$). As was shown in [13], small source-detector separations of the order of one lattice step h are sufficient to break the symmetry and eliminate the false images. If both absorbing and diffusing inhomogeneities are present, at least two detectors per source are required to make the problem well determined.

The paraxial methods are attractive due to their experimental simplicity. Indeed, instead of independently scanning the sources and detectors over the measurement planes, as is required in both the Fourier and real-space methods, in the paraxial measurement scheme one only needs to scan a fixed source-detector "arm" as is illustrated in Fig. 4.

4. Plane-wave illumination scheme

An especially simple reconstruction algorithm is obtained in the case when for each location of the source the output of all possible detectors is summed. Experimentally, this can be achieved with the use of a lens to either collect the outgoing radiation or to illuminate the medium. Both approaches are mathematically identical due to source-detector reciprocity. Obviously, this method can be applied only in the transmission geometry, similar to the paraxial and coaxial methods. The plane wave illumination scheme was first proposed in [20] for time-resolved diffuse tomography; here, we show that this method is a particular case of the phased-array measurement scheme which is discussed in Sec. III A.

We will consider a point source which is scanned over the measurement plane $x=-L/2$ and an integrating detector at $x=L/2$ which measures the quantity $\int d^2\rho_d\phi(\omega,\boldsymbol{\rho}_s,\boldsymbol{\rho}_d)$. Accordingly, the summation in Eq. (40) over discrete values of $\Delta\boldsymbol{\rho}_j$ must be replaced by an integration over $d^2\Delta\rho$ and the coefficients c_{ij} replaced by unity. This results in a simple

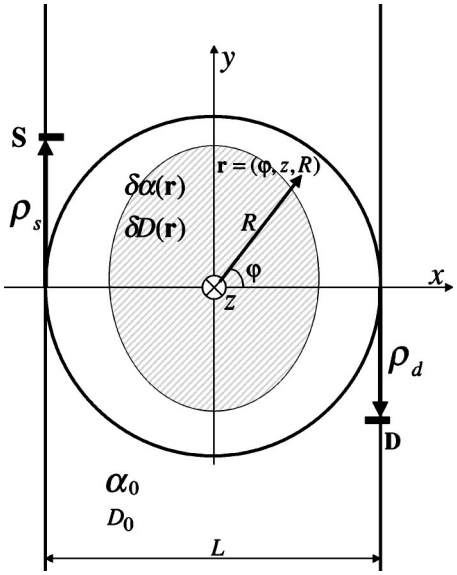

FIG. 5. Sketch of the experimental setup and the coordinate system for the planar geometry with rotations (transmission measurements).

expression for $K(\omega,\mathbf{q};x)$ which is now independent of the variable i:

$$K(\omega,\mathbf{q};x)=\kappa(\omega,\mathbf{q},0;x). \tag{79}$$

Similarly, the kernel Γ defined by Eq. (39) becomes independent of i: $\Gamma=\Gamma(\omega,\boldsymbol{\rho}_s;\mathbf{r})$.

It can be seen that the numerical evaluation of the functions K which is required in both real-space and paraxial modalities is altogether avoided. Reconstructed images are obtained by a straightforward application of the inversion formula (63) where $\mu=\omega$ and, similarly to the coaxial and paraxial imaging schemes, multiple modulation frequencies must be employed.

IV. PLANAR GEOMETRY WITH ROTATIONS

The spatial resolution of images reconstructed in the planar geometry has been shown to be different in the directions parallel and perpendicular to the measurement planes [10–13]. The transverse resolution is limited by the step size of the lattice on which the sources are placed. However, the depth resolution is, generally, lower and is much more strongly influenced by noise. The low depth resolution is not a characteristic only of the planar measurement scheme. A similar problem was observed in the cylindrical geometry [14], and we expect that the depth resolution will remain low for measurements taken on any closed surface. In this section we propose a method aimed at improving the depth resolution. The method involves rotating two parallel measurement planes around the inhomogenieties of the medium. Although the reconstruction algorithm will be ultimately formulated in cylindrical coordinates, the method discussed in this section is not equivalent to taking measurements on the surface of a cylinder (see Sec. V).

A sketch of the proposed experiment is shown in Fig. 5. Here the medium is placed inside a cylinder of radius $L/2$ whose axis coincides with the z axis. As in the previous section, the measurements are taken on the surface of two parallel planes which touch the surface of the cylinder and can rotate around its axis. The space between the measurement planes is filled with a homogeneous matching medium while the inhomogeneities are located in the region $R<L/2$. It is important to emphasize that the boundary conditions are imposed on the surface of the planes rather than on the surface of the cylinder and that the inhomogeneities inside the cylinder are assumed to not be disturbed as a result of the rotation. We treat the measurements obtained for different rotation angles θ as a single set of data and obtain an SVD pseudoinverse solution for the unknown optical coefficients.

We start with reformulating the integral Eq. (43) in appropriate coordinates. Namely, we use cylindrical coordinates φ,z,R such that $x=R\cos\varphi$ and $y=R\sin\varphi$. For a given fixed orientation of the measurement planes with respect to the medium, one can write

$$\phi(\mu,\boldsymbol{\rho}_s)=\int_0^{2\pi}d\varphi\int_{-\infty}^{\infty}dz\int_0^{L/2}\times RdR\,\Gamma(\mu,\boldsymbol{\rho}_s;\varphi,z,R)\,\eta(\varphi,z,R), \tag{80}$$

where the kernel Γ is given by

$$\Gamma(\mu,\boldsymbol{\rho}_s;\varphi,z,R)=\int\frac{dq_y dq_z}{(2\pi)^2}K(\mu,q_y,q_z;R\cos\varphi)\times\exp[iq_y(R\sin\varphi-y_s)]\exp[iq_z(z-z_s)]. \tag{81}$$

Since the kernel Γ is periodic in the variable φ, we can expand it into a Fourier series according to

$$\Gamma(\mu,\boldsymbol{\rho}_s;\varphi,z,R)=\sum_{m=-\infty}^{\infty}\int\frac{dq_y dq_z}{(2\pi)^3}a(\mu,q_y,q_z,m;R)\times\exp[i(m\varphi-q_y y_s)+iq_z(z-z_s)], \tag{82}$$

where

$$a(\mu,q_y,q_z,m;R)=\int_0^{2\pi}K(\mu,q_y,q_z;R\cos\varphi)\times\exp[i(q_yR\sin\varphi-m\varphi)]d\varphi. \tag{83}$$

Now we rotate the measurement planes by an angle θ (measured in the laboratory frame) around the axis of the cylinder. The data function obviously depends on θ and we consider this variable as an additional degree of freedom. Equation (80) is transformed according to

$$\phi(\mu,\boldsymbol{\rho}_s,\theta)=\int_0^{2\pi}d\varphi\int_{-\infty}^{\infty}dz\int_0^{L/2}RdR\Gamma(\mu,\boldsymbol{\rho}_s,\theta;\varphi,z,R)\times\eta(\varphi,z,R), \tag{84}$$

with

$$\Gamma(\mu,\boldsymbol{\rho}_s,\theta;\varphi,z,R)=\sum_{m=-\infty}^{\infty}\int\frac{dq_y dq_z}{(2\pi)^3}a(\mu,q_y,q_z,m;R)\times\exp[im(\varphi-\theta)-iq_y y_s+iq_z(z-z_s)]. \tag{85}$$

It can be seen from the structure of the kernel Γ that it is translationally invariant in the variables φ and z but not in y. Therefore, the variable y_s can be considered as an "internal" degree of freedom. If y_s is sampled on an infinite lattice, we can construct an analog of the Fourier method discussed in Sec. III C 1 with the variable y_s taking the place of $\Delta\boldsymbol{\rho}$. In this section such a pseudoinverse solution will be constructed. However, a more general case can be considered when y_s does not lie on a lattice but takes a finite number of discrete values. This approach corresponds to the real-space method (Sec. III C 2) and is discussed in the Appendix.

Here we assume that, as in the rest of the paper, both y_s and z_s lie on a square lattice with step size h. We also assume that the rotation angles θ take the values $\theta_j=2\pi(j-1)/N_\theta$, $j=1,2,\ldots,N_\theta$. However, no assumptions about the detectors are made at this point. The inversion formulas are derived analogously to the case of a fixed geometry discussed in Sec. III B. First, we calculate the matrix elements of the operator $\Gamma\Gamma^*$. A straightforward calculation shows that

$$\langle\mu\boldsymbol{\rho}_s\theta|\Gamma\Gamma^*|\mu'\boldsymbol{\rho}_s'\theta'\rangle=\sum_{m=-\infty}^{\infty}\int\frac{dq_y dq_y' dq_z}{(2\pi)^4}\langle\mu q_y|\tilde{M}_1(q_z,m)|\mu' q_y'\rangle\times\exp[-i(q_y y_s-q_y' y_s')-iq_z(z_s-z_s')-im(\theta-\theta')], \tag{86}$$

where

$$\langle\mu q_y|\tilde{M}_1(q_z,m)|\mu' q_y'\rangle=\int_0^{L/2}RdR\;a(\mu,q_y,q_z,m;R)a^*(\mu',q_y',q_z,m;R). \tag{87}$$

The eigenfunctions of $\Gamma\Gamma^*$, Eq. (86), are

$$\langle\mu\boldsymbol{\rho}_s\theta|f_{u_z n\lambda}\rangle=\frac{h\exp[-i(u_z z_s+n\theta)]}{2\pi\sqrt{N_\theta}}\int_{-\pi/h}^{\pi/h}du_y\exp(-iu_y y_s)\times\langle\mu u_y|C_\lambda(u_z,n)\rangle, \tag{88}$$

where $u_z\in[-\pi/h,\pi/h]$, $n=1,2,\ldots,N_\theta$, and $|C_\lambda(u_z,n)\rangle$ are the eigenfunctions of the operator $\tilde{M}(u_z,n)$ which has a smaller dimensionality than $\Gamma\Gamma^*$ and is defined by

$$\langle\mu u_y|\tilde{M}(u_z,n)|\mu' u_y'\rangle=\sum_{k=-\infty}^{\infty}\sum_{v_y,v_y'}\sum_{v_z}\times\langle\mu,u_y+v_y|\tilde{M}_1(u_z+v_z,n+N_\theta k)|\mu',u_y'+v_y'\rangle. \tag{89}$$

Here $u_y,u_y',u_z\in[-\pi/h,\pi/h]$, v_y,v_y', and v_z are one-dimensional reciprocal lattice vectors. We denote the eigenvalues of the non-negative definite operator $\tilde{M}(u_z,n)$ by $M_\lambda^2(u_z,n)$:

$$\tilde{M}(u_z,n)|C_\lambda(u_z,n)\rangle=M_\lambda^2(u_z,n)|C_\lambda(u_z,n)\rangle. \tag{90}$$

The singular values of the problem, $\sigma_{u_z n\lambda}$, are the eigenvalues of the operator $\Gamma\Gamma^*$. It can be verified by direct calculation that

$$\Gamma\Gamma^*|f_{u_z n\lambda}\rangle=\sigma_{u_z n\lambda}^2|f_{u_z n\lambda}\rangle, \tag{91}$$

where

$$\sigma_{u_z n\lambda}^2=\frac{N_\theta M_\lambda^2(u_z,n)}{(2\pi h)^2}. \tag{92}$$

The second set of singular functions, $|g_{u_z n\lambda}\rangle$, can be found from the relation $\sigma_{u_z n\lambda}|g_{u_z n\lambda}\rangle=\Gamma^*|f_{u_z n\lambda}\rangle$. The result is given by

$$\langle\varphi zR|g_{u_z n\lambda}\rangle=\frac{\sqrt{N_\theta}\exp[-i(u_z z+n\varphi)]}{2\pi h\sigma_{u_z n\lambda}}\sum_\mu\int_{-\pi/h}^{\pi/h}du_y\times\tilde{P}^*(\mu,\mathbf{u};\varphi,R)\langle\mu u_y|C_\lambda(u_z,n)\rangle, \tag{93}$$

where

$$\tilde{P}(\mu,\mathbf{u},n;\varphi,z,R)=\sum_{k=-\infty}^{\infty}\sum_{\mathbf{v}}a(\mu,\mathbf{u}+\mathbf{v},n+N_\theta k;R)\times\exp(iN_\theta k\varphi+iv_z z). \tag{94}$$

Next, we apply the definitions of the pseudoinverse solution (45) and (47). Omitting intermediate steps, we obtain the following inversion formula:

$$\eta(\mathbf{r})=\frac{h^2}{N_\theta}\sum_{n=1}^{N_\theta}\int_{-\pi/h}^{\pi/h}du_z\exp[-i(u_z z+n\varphi)]\times\sum_{\mu,\mu'}\int_{-\pi/h}^{\pi/h}du_y\int_{-\pi/h}^{\pi/h}du_y'\tilde{P}^*(\mu,\mathbf{u},n;\varphi,z,R)\times\langle\mu u_y|\tilde{M}^{-1}(u_z,n)|\mu' u_y'\rangle\tilde{\phi}(\mu',u_y',u_z,n), \tag{95}$$

where

$$\tilde{\phi}(\mu;\mathbf{u},n)=\sum_{\boldsymbol{\rho}_s,\theta}\phi(\mu,\boldsymbol{\rho}_s,\theta)\exp[i(\mathbf{u}\cdot\boldsymbol{\rho}_s+n\theta)] \tag{96}$$

is the Fourier-transformed data function.

As in Sec. III C 1 we can discretize the variable u_y. In this case M becomes a finite matrix which can be diagonalized by the usual methods of linear algebra. The discrete variable u_y is an "internal" degree of freedom and it is logical to include it in the composite variable μ: $\mu=(\omega,\Delta\boldsymbol{\rho},u_y)$. Then the inversion formula can be compactly written as

$$\eta(\mathbf{r}) = \frac{h^2}{N_\theta}\sum_{n=1}^{N_\theta}\int_{-\pi/h}^{\pi/h} du_z \exp[-i(u_z z + n\varphi)] \times \sum_{\mu,\mu'} P^*(\mu,u_z,n;\varphi,z,R)\langle\mu|\tilde{M}^{-1}(u_z,n)|\mu'\rangle \times \tilde{\phi}(\mu',u_z,n). \quad (97)$$

It may seem that the angular resolution of the reconstructed images is limited by $2\pi/N_\theta$ since Eq. (97) contains only factors $\exp(-in\varphi)$ with $n=1,2,\ldots,N_\theta$. However, this is not so. In fact, the functions $P(\mu,u_z,n;\varphi,z,R)$ also depend on φ [see Eq. (94)]. The product $\exp(-in\varphi)P^*(\mu,u_z,n;\varphi,z,R)$ contains the modes $\exp(-im\varphi)$ with arbitrary m. Therefore, at least theoretically, the angular resolution of the inversion formula (97) is not limited, even if only a small number of rotations is used. In the limit $N_\theta=1$, Eq. (97) becomes equivalent to the reconstruction formula (77) for the geometry without rotations. The first nontrivial case $N_\theta=2$ corresponds to the rotation of the measurement planes by the angle π. Such a rotation can, in principle, provide additional data (except for purely coaxial measurements), but is not expected to produce a significant increase in the depth resolution. Indeed, in the $N_\theta=2$ case the x axis is always perpendicular to the measurement planes. One can expect that the depth resolution will dramatically increase for $N_\theta=4$. In this case, the x axis is perpendicular to the measurement planes for $\theta_1=0$ and $\theta_3=\pi$. However, it is parallel to the measurement planes for $\theta_2=\pi/2$ and $\theta_4=3\pi/2$. Thus, the x and y directions become completely equivalent, and one can expect to achieve the fundamental resolution limit of one lattice step in all three dimensions.

To conclude this section, we note that the analysis of the special cases discussed in Sec. III C can be applied with rotations, with one exception. Namely, if $N_\theta>2$, the symmetry with respect to the plane $x=0$ that resulted in twinned images for the purely coaxial measurement scheme is no longer present. Therefore, the coaxial method can be used in conjunction with rotations if only absorbing inhomogeneities are present. However, if both absorbing and scattering inhomogeneities are present, at least two detectors per source must be used.

V. CYLINDRICAL GEOMETRY

The cylindrical geometry is illustrated in Fig. 6. The data function is measured on an infinite surface $R=L/2$, where we have used cylindrical coordinates $\mathbf{r}=(\varphi,z,R)$. The data function can be written as $\phi=\phi(\omega,\varphi_s,z_s,\varphi_d,z_d)$, where (φ_s,z_s) characterize the location of the source and (φ_d,z_d) the location of the detector. The data function satisfies the integral equation

$$\phi(\omega,\varphi_s,z_s,\varphi_d,z_d) = \int_0^{2\pi} d\varphi \int_{-\infty}^{\infty} dz \int_0^{L/2} RdR \times \Gamma(\omega,\varphi_s,z_s,\varphi_d,z_d;\varphi,z,R)\,\eta(\varphi,z,R). \quad (98)$$

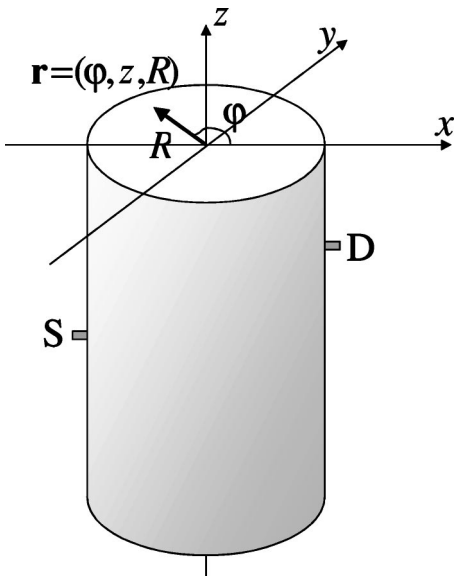

FIG. 6. Sketch of the experimental setup in the cylindrical geometry.

The invariance of the unperturbed medium with respect to translations along and rotations about the z axis requires that the kernel Γ have a Fourier expansion of the form

$$\Gamma(\omega,\varphi_s,z_s,\varphi_d,z_d;\varphi,z,R) = \sum_{m_s,m_d}\int \frac{dq_s dq_d}{(2\pi)^4}\kappa(\omega,m_s,q_s,m_d,q_d;R)\exp[iq_s(z-z_s) + iq_d(z_d-z) + im_s(\varphi-\varphi_s) + im_d(\varphi_d-\varphi)]. \quad (99)$$

As in the case of planar measurements, we introduce the new variables Δz, $\Delta\varphi$, q, p, m, and n according to $z_d=z_s+\Delta z$, $\varphi_d=\varphi_s+\Delta\varphi$, $q_s=q+p$, $q_d=p$, $m_s=m+n$, and $m_d=n$. We also introduce the composite variable μ, which in the case of the cylindrical geometry has the form $\mu=(\omega,\Delta\varphi,\Delta z)$. Then the kernel Γ acquires the form

$$\Gamma(\mu,\varphi_s,z_s;\varphi,z,R) = \sum_m \int \frac{dq}{(2\pi)^2} K(\mu,q,m;R) \times \exp[im(\varphi-\varphi_s) + iq(z-z_s)], \quad (100)$$

where

$$K(\mu,q,m;R) = \sum_n \int \frac{dp}{(2\pi)^2}\kappa(\omega,m+n,q+p,n,p;R) \times \exp[i(p\Delta z + n\Delta\varphi)]. \quad (101)$$

Further derivations are very similar to those performed for the geometry in Sec. III B. The only difference is that the variable y which in the case of an infinite medium varies from $-\infty$ to ∞ is replaced by φ which now varies from 0 to 2π. To construct an inversion formula, we assume that z_s is on an infinite one-dimensional lattice with step h while φ_s takes the values $2\pi(j-1)/N_\varphi$, $j=1,2,\ldots,N_\varphi$, and consider the eigenfunctions and eigenvalues of the operator $\Gamma\Gamma^*$.

Omitting intermediate calculations, we obtain the final result (analogous to Eq. (63) for the planar geometry)

$$\eta(\mathbf{r}) = h\sum_{n=1}^{N_\varphi}\int_{-\pi/h}^{\pi/h}\frac{du}{(2\pi)^2}\exp[-i(uz+n\varphi)]\sum_{\mu,\mu'}P^*(\mu,n,u;\mathbf{r}) \times\langle\mu|M^{-1}(n,u)|\mu'\rangle\tilde{\phi}(\mu',n,u). \quad (102)$$

Here

$$P(\mu,n,u;\mathbf{r}) = \sum_{k=-\infty}^{\infty}\sum_{v}K(\mu,u+v,n+N_\varphi k;R) \times\exp\left[i(vz+N_\varphi k\varphi)\right], \quad (103)$$

$$M(n,u) = \sum_{k=-\infty}^{\infty}\sum_{v}M_1(n+N_\varphi k,u+v), \quad (104)$$

$$\langle\mu|M_1(m,q)|\mu'\rangle = \int_0^{L/2}K(\mu,q,m;R)K^*(\mu',q,m;R)RdR, \quad (105)$$

$$\tilde{\phi}(\mu,n,u) = \sum_{\varphi_s,z_s}\phi(\mu,\varphi_s,z_s)\exp\left[i(n\varphi_s+uz_s)\right]. \quad (106)$$

The analysis which applies to the inversion formulas in the planar geometry is also applicable to Eq. (102) . For example, the inverse matrix $M^{-1}(n,u)$ must be appropriately regularized. The inversion formula (102) corresponds to the real-space method in the plane geometry. However, other special cases can be also considered. If either $\Delta\varphi$ or Δz or both lie on a lattice (which would require that the detectors are placed on a lattice which is a subset of the lattice of the sources), the Fourier method discussed in Sec. III C 1 can be applied. The paraxial measurement scheme (Sec. III C 3) corresponds to the case when only a few values of $\Delta\varphi=\pi+\delta\varphi$ and Δz are used (where $\delta\varphi\ll\pi$ and $\Delta z\ll L/2$) in conjunction with multiple modulation frequencies. In the coaxial case a symmetry is present in Eq. (98) with respect to rotation of $\eta(\mathbf{r})$ by the angle π around the z axis. This symmetry would result in the appearance of artifacts in the reconstructed images. The problem is solved by the use of off-axis data.

The only special case discussed in Sec. III C that cannot be considered in the cylindrical geometry is the plane-wave detection-illumination (Sec. III C 4) experiment. This follows from the fact that one can not integrate the detector output over all values of $\Delta\varphi$ and Δz (which will necessarily include the location of the source). In the planar geometry the sources and detectors can be placed on different planes which do not intersect. This is not the case in the cylindrical geometry. While it is possible to achieve similar mathematical simplifications by integrating the source and detector outputs over angles, when $z_s\neq z_d$ (physically, this corresponds to ring rather than pointlike sources and detectors), this will lead to a complete loss of angular resolution in the reconstructed images. Similarly, integration of the source and detector outputs along lines parallel to the cylinder axis and characterized by different angles $\varphi_s\neq\varphi_d$ will result in a complete loss of z resolution.

VI. EXAMPLES OF CALCULATING THE KERNELS

In this section we present several examples of calculating the kernel Γ which appears in the integral equations (32) and (98) and the related functions κ appearing in the Fourier expansions of Γ Eqs. (35) and (99). In the case of the DE we use boundary conditions given by Eq. (18). We also provide an analytic expression for Γ within the RTE forward model. In the case of the RTE, we assume free boundaries (G_0 is calculated in an infinite medium) and assume that the phase function $A(\hat{\mathbf{s}},\hat{\mathbf{s}'})$ is constant (isotropic scattering).

Note that, as discussed in Sec. II, regardless of the linearization method used, the integral equation that relates the unknown operator V to the measurable data function is given by Eq. (25). Thus, to obtain expressions for κ, we must calculate the unperturbed Green's functions for the DE or RTE in appropriate coordinates.

A. Diffusion approximation: Planar geometry

In the planar geometry, the unperturbed Green's function can be written as [21]

$$G_0(\mathbf{r},\mathbf{r}') = \int\frac{d^2q}{(2\pi)^2}g(\mathbf{q};x,x')\exp[i\mathbf{q}\cdot(\boldsymbol{\rho}'-\boldsymbol{\rho})]. \quad (107)$$

Substituting this expression into the integral equation (25), where the operator V is defined by Eq. (21), and using the definition of the functions κ Eq. (35), we find that $\kappa=(\kappa_\alpha,\kappa_D)$ is expressed in terms of the functions g as

$$\kappa_\alpha(\omega,\mathbf{q}_s,\mathbf{q}_d;x) = \left(1+\frac{\ell^*}{\ell}\right)^2 g(\mathbf{q}_s;x_s,x)g(\mathbf{q}_d;x,x_d), \quad (108)$$

$$\kappa_D(\omega,\mathbf{q}_s,\mathbf{q}_d;x) = \left(1+\frac{\ell^*}{\ell}\right)^2\left[\mathbf{q}_s\cdot\mathbf{q}_d g(\mathbf{q}_s;x_s,x)g(\mathbf{q}_d;x,x_d) + \frac{\partial g(\mathbf{q}_s;x_s,x)}{\partial x}\frac{\partial g(\mathbf{q}_d;x,x_d)}{\partial x}\right]. \quad (109)$$

Here an implicit dependence of the functions g on the modulation frequency ω is implied.

Thus, it is sufficient to find the functions g which satisfy the DE (20) and the boundary conditions (18). Substituting Eq. (107) into Eq. (20), we find that $g(\mathbf{q};x,x')$ must satisfy the one-dimensional equation

$$\left[\frac{\partial^2}{\partial x^2}-Q^2(\mathbf{q})\right]g(\mathbf{q};x,x') = -\frac{\delta(x-x')}{D_0}, \quad (110)$$

where

$$Q(\mathbf{q}) = (q^2+k^2)^{1/2} \quad (111)$$

and the diffuse wave number k is given by $k^2=(\alpha_0-i\omega)/D_0$.

It follows from Eq. (110) that the function g is a linear combination of exponentials $\exp(\pm Qx)$ with coefficients depending on x'. It is continuous at $x=x'$ but its first derivative experiences a discontinuity at this point:

$$g(\mathbf{q};x'+0,x') - g(q;x'-0,x') = 0, \tag{112}$$

$$g'(\mathbf{q};x'+0,x') - g'(\mathbf{q};x'-0,x') = -1/D_0. \tag{113}$$

In addition, the boundary conditions (18) at $x=\pm L/2$ read

$$g(\mathbf{q};-L/2,x') - \ell g'(\mathbf{q};-L/2,x') = 0, \tag{114}$$

$$g(\mathbf{q};L/2,x') + \ell g'(\mathbf{q};L/2,x') = 0, \tag{115}$$

where the prime denotes differentiation with respect to x. The conditions (112)–(115) lead to the following expression for g:

$$g(\mathbf{q};x,x') = \frac{[1+(Q\ell)^2]\cosh[Q(L-|x-x'|)] - [1-(Q\ell)^2]\cosh[Q(x+x')] + 2Q\ell\sinh[Q(L-|x-x'|)]}{2D_0Q[\sinh(QL) + 2Q\ell\cosh(QL) + (Q\ell)^2\sinh(QL)]}. \tag{116}$$

This expression can be simplified if we take into account that in Eq. (25) one of the arguments of the Green's functions ($\mathbf{r}$ or $\mathbf{r}'$) must be on the boundary. Thus, it is enough to consider the above expression in the limit when either $x=\pm L/2$ or $x'=\pm L/2$. It can be seen that these two limits are given by the same expression—namely,

$$g(\mathbf{q};x,x')_{x=\pm L/2} = g(\mathbf{q};x,x')_{x'=\pm L/2} = \frac{\ell}{D_0} g_b(\mathbf{q};x,x'), \tag{117}$$

where

$$g_b(\mathbf{q};x,x') = \frac{\sinh[Q(L-|x-x'|)] + Q\ell\,\cosh[Q(L-|x-x'|)]}{\sinh(QL) + 2Q\ell\,\cosh(QL) + (Q\ell)^2\sinh(QL)}. \tag{118}$$

Now the functions κ can be expressed in terms of the functions g_b as

$$\kappa_\alpha(\omega,\mathbf{q}_s,\mathbf{q}_d;x) = \left(\frac{\ell+\ell^*}{D_0}\right)^2 g_b(\mathbf{q}_s;x_s,x) g_b(\mathbf{q}_d;x,x_d), \tag{119}$$

$$\kappa_D(\omega,\mathbf{q}_s,\mathbf{q}_d;x) = \left(\frac{\ell+\ell^*}{D_0}\right)^2 \left[\mathbf{q}_s\cdot\mathbf{q}_d g_b(\mathbf{q}_s;x_s,x) g_b(\mathbf{q}_d;x,x_d) + \frac{\partial g_b(\mathbf{q}_s;x_s,x)}{\partial x}\frac{\partial g_b(\mathbf{q}_d;x,x_d)}{\partial x}\right]. \tag{120}$$

The above expressions are well defined in the limits $\ell\to 0$ and $\ell\to\infty$. For example, for purely absorbing boundaries ($\ell=0$) and in the transmission geometry ($x_s=-L/2$ and $x_d=L/2$), we obtain

$$\kappa_\alpha(\omega,\mathbf{q}_s,\mathbf{q}_d;x) = \left(\frac{\ell^*}{D_0}\right)^2 \frac{\sinh[Q(\mathbf{q}_s)(L/2-x)]\sinh[Q(\mathbf{q}_d)(L/2+x)]}{\sinh[Q(\mathbf{q}_s)L]\sinh[Q(\mathbf{q}_d)L]}, \tag{121}$$

$$\kappa_D(\omega,\mathbf{q}_s,\mathbf{q}_d;x) = \left(\frac{\ell^*}{D_0}\right)^2 \left[-\frac{Q(\mathbf{q}_s)Q(\mathbf{q}_d)\cosh[Q(\mathbf{q}_s)(L/2-x)]\cosh[Q(\mathbf{q}_d)(L/2+x)]}{\sinh[Q(\mathbf{q}_s)L]\sinh[Q(\mathbf{q}_d)L]} + \frac{\mathbf{q}_s\cdot\mathbf{q}_d\sinh[Q(\mathbf{q}_s)(L/2-x)]\sinh[Q(\mathbf{q}_d)(L/2+x)]}{\sinh[Q(\mathbf{q}_s)L]\sinh[Q(\mathbf{q}_d)L]}\right]. \tag{122}$$

In the opposite limit of purely reflecting boundaries, we obtain

$$\kappa_\alpha(\omega,\mathbf{q}_s,\mathbf{q}_d;x) = \frac{\cosh[Q(\mathbf{q}_s)(L/2-x)]\cosh[Q(\mathbf{q}_d)(L/2+x)]}{D_0^2 Q(\mathbf{q}_s)Q(\mathbf{q}_d)\sinh[Q(\mathbf{q}_s)L]\sinh[Q(\mathbf{q}_s)L]}, \tag{123}$$

$$\kappa_D(\omega,\mathbf{q}_s,\mathbf{q}_d;x) = \frac{1}{D_0^2}\left[-\frac{\sinh[Q(\mathbf{q}_s)(L/2-x)]\sinh[Q(\mathbf{q}_d)(L/2+x)]}{\sinh[Q(\mathbf{q}_s)L]\sinh[Q(\mathbf{q}_d)L]} + \frac{\mathbf{q}_s\cdot\mathbf{q}_d\cosh[Q(\mathbf{q}_s)(L/2-x)]\cosh[Q(\mathbf{q}_d)(L/2+x)]}{Q(\mathbf{q}_s)Q(\mathbf{q}_d)\sinh[Q(\mathbf{q}_s)L]\sinh[Q(\mathbf{q}_d)L]}\right]. \tag{124}$$

B. Diffusion approximation: Cylindrical geometry

In the cylindrical geometry we use the following expansion for the unperturbed Green's function [21]:

$$G_0(\mathbf{r},\mathbf{r}') = \sum_{m=-\infty}^{\infty} \int \frac{dq}{(2\pi)^2} \exp[im(\varphi-\varphi')] \times \exp[iq(z-z')] g(m,q;R,R'). \quad (125)$$

We can express the functions κ appearing in Eq. (99) in terms of the functions g defined above as

$$\kappa_\alpha(\omega,m_s,q_s,m_d,q_d;R) = \left(1+\frac{\ell^*}{\ell}\right)^2 g(m_s,q_s;L/2,R) \times g(m_d,q_d;R,L/2), \quad (126)$$

$$\kappa_D(\omega,m_s,q_s,m_d,q_d;R) = \left(1+\frac{\ell^*}{\ell}\right)^2 \left[\frac{\partial g(m_s,q_s;L/2,R)}{\partial R} \frac{\partial g(m_d,q_d;R,L/2)}{\partial R} + \left(q_s q_d + \frac{m_s m_d}{R^2}\right) g(m_s,q_s;L/2,R) g(m_d,q_d;R,L/2) \right]. \quad (127)$$

Here we used the fact that for both sources and detectors, $R_s = R_d = L/2$.

Upon substitution of Eq. (125) into the DE (20), we find that $g(m,q;R,R')$ must satisfy the one-dimensional equation

$$\left[\frac{1}{R}\frac{\partial}{\partial R} R \frac{\partial}{\partial R} - \frac{m^2}{R^2} - Q^2(q)\right] g(m,q;R,R') = -\frac{\delta(R-R')}{D_0 R}. \quad (128)$$

The solution to Eq. (125) is given by a combination of modified Bessel and Hankel functions of the first kind, $I_m(QR)$ and $K_m(QR)$, and is subject to the following conditions:

$$g(m,q;0,R') < \infty, \quad (129)$$

$$g(m,q;R'+0,R') - g(m,q;R'-0,R') = 0, \quad (130)$$

$$g'(m,q;R'+0,R') - g'(m,q;R'-0,R') = -1/D_0 R', \quad (131)$$

$$g(m,q;L/2,R') + \ell g'(m,q;L/2,R') = 0. \quad (132)$$

The solution that satisfies the above conditions is

$$g(m,q;R,R') = \frac{1}{D_0}\left[K_m(QR_>) I_m(QR_<) - \frac{K_m(QL/2)+Q\ell K_m'(QL/2)}{I_m(QL/2)+Q\ell I_m'(QL/2)} \times I_m(QR) I_m(QR') \right], \quad (133)$$

where $R_>$ and $R_<$ are the greater and lesser of R and R'. On the measurement surface Eq. (133) becomes

$$g(m,q;\rho,L/2) = g(m,q;L/2,R) = \frac{\ell}{D_0} g_b(m,q;R), \quad (134)$$

where

$$g_b(m,q;R) = \frac{2}{L}\frac{I_m(QR)}{I_m(QL/2)+Q\ell I_m'(QL/2)}. \quad (135)$$

Now we can express the kernel κ in terms of the simpler functions g_b as follows:

$$\kappa_\alpha(\omega,m_s,q_s,m_d,q_d;R) = \left(\frac{\ell+\ell^*}{D_0}\right)^2 g_b(m_s,q_s;R) g_b(m_d,q_d;R), \quad (136)$$

$$\kappa_D(\omega,m_s,q_s,m_d,q_d;R) = \left(\frac{\ell+\ell^*}{D_0}\right)^2 \left[\frac{\partial g_b(m_s,q_s;R)}{\partial R} \frac{\partial g_b(m_d,q_d;R)}{\partial R} + \left(q_s q_d + \frac{m_s m_d}{R^2}\right) g_b(m_s,q_s;R) g_b(m_d,q_d;R) \right]. \quad (137)$$

Again, the above expression is well defined in the limits $\ell \to 0$ and $\ell \to \infty$. Thus, for example, for absorbing boundaries, we have

$$\kappa_\alpha(\omega,m_s,q_s,m_d,q_d;R) = \left(\frac{2\ell^*}{D_0 L}\right)^2 \frac{I_{m_s}[Q(q_s)R] I_{m_d}[Q(q_d)R]}{I_{m_s}[Q(q_s)L/2] I_{m_d}[Q(q_d)L/2]}, \quad (138)$$

$$\kappa_D(\omega,m_s,q_s,m_d,q_d;R) = \left(\frac{2\ell^*}{D_0 L}\right)^2 \left[\frac{Q(q_s)Q(q_d) I_{m_s}'[Q(q_s)R] I_{m_d}'[Q(q_d)R]}{I_{m_s}[Q(q_s)L/2] I_{m_d}[Q(q_d)L/2]} + \left(q_s q_d + \frac{m_s m_d}{R^2}\right) \frac{I_{m_s}[Q(q_s)R] I_{m_d}[Q(q_d)R]}{I_{m_s}[Q(q_s)L/2] I_{m_d}[Q(q_d)L/2]} \right]. \quad (139)$$

In the case of reflecting boundaries ($\ell \to \infty$), the analogous expressions are

$$\kappa_\alpha(\omega,m_s,q_s,m_d,q_d;R) = \left(\frac{2}{D_0 L}\right)^2 \frac{I_{m_s}[Q(q_s)R]I_{m_d}[Q(q_d)R]}{Q(q_s)Q(q_d)I'_{m_s}[Q(q_s)L/2]I'_{m_d}[Q(q_d)L/2]}, \tag{140}$$

$$\kappa_D(\omega,m_s,q_s,m_d,q_d;R) = \left(\frac{2}{D_0 L}\right)^2 \left[\frac{I'_{m_s}[Q(q_s)R]I'_{m_d}[Q(q_d)R]}{I'_{m_s}[Q(q_s)L/2]I'_{m_d}[Q(q_d)L/2]} + \frac{R^2 q_s q_d + m_s m_d}{R^2 Q(q_s)Q(q_d)} \frac{I_{m_s}[Q(q_s)R]I_{m_d}[Q(q_d)R]}{I'_{m_s}[Q(q_s)L/2]I'_{m_d}[Q(q_d)L/2]} \right]. \tag{141}$$

C. Beyond the diffusion approximation

Consider Eq. (9) in an infinite medium with isotropic scattering. In this case the unperturbed Green's function can be obtained [22] as a three-dimensional Fourier integral:

$$G_0(\mathbf{r},\hat{\mathbf{s}};\mathbf{r}',\hat{\mathbf{s}}') = \int \frac{d^3k}{(2\pi)^3} \exp[i\mathbf{k}\cdot(\mathbf{r}'-\mathbf{r})] \left[\frac{\delta(\hat{\mathbf{s}}-\hat{\mathbf{s}}')}{\mu_t - i\mathbf{k}\cdot\hat{\mathbf{s}}} + \frac{\mu_s/4\pi}{(\mu_t - i\mathbf{k}\cdot\hat{\mathbf{s}})(\mu_t - i\mathbf{k}\cdot\hat{\mathbf{s}}')\left(1 - \frac{\mu_s}{k}\arctan\frac{k}{\mu_t}\right)} \right]. \tag{142}$$

The first term in the square brackets corresponds to "ballistic" photons and decays exponentially on the scale of $1/\mu_t$. We will ignore this term below. The second term accounts for diffuse (multiply scattered) photons.

We consider the slab geometry with the measurement planes located at $x=x_s=-L/2$ and $x=x_d=L/2$. By expanding the three-dimensional vector $\mathbf{k}$ as $\mathbf{k}=k_x\hat{\mathbf{x}}+\mathbf{q}$ where $\hat{\mathbf{x}}\cdot\mathbf{q}=0$, we can rewrite Eq. (142) as

$$G_0(\mathbf{r},\hat{\mathbf{s}};\mathbf{r}',\hat{\mathbf{s}}') = \int \frac{d^2q}{(2\pi)^2} g(\mathbf{q};x,\hat{\mathbf{s}};x',\hat{\mathbf{s}}') \exp[i\mathbf{q}\cdot(\boldsymbol{\rho}'-\boldsymbol{\rho})], \tag{143}$$

where

$$g(\mathbf{q};x,\hat{\mathbf{s}};x',\hat{\mathbf{s}}') = \int_{-\infty}^{\infty} \frac{dk_x}{2\pi} \frac{\exp[ik_x(x'-x)]}{[\mu_t - i(\mathbf{q}+k_x\hat{\mathbf{x}})\cdot\hat{\mathbf{s}}][\mu_t - i(\mathbf{q}+k_x\hat{\mathbf{x}})\cdot\hat{\mathbf{s}}']\left[1 - \frac{\mu_s}{\sqrt{q^2+k_x^2}}\arctan\frac{\sqrt{q^2+k_x^2}}{\mu_t}\right]}. \tag{144}$$

Now recall that in Sec. I B the perturbation was defined by $V=\delta\mu^* - \delta\mu_s' A'$. However, the above expressions solution depends on $\mu_a=\mu_t-\mu_s$ and μ_s directly. Therefore, it is more convenient to consider μ_a and μ_s as independent. For simplicity, we assume that $\delta\mu_s=0$ and $\omega=0$ (cw case). Then $V=\delta\mu^*=\delta\mu_a$, and the integral equation relating the measurable data to $\delta\mu_a$ takes the form (32) where $\Gamma(\boldsymbol{\rho}_s,\boldsymbol{\rho}_d;\mathbf{r})$ is given by Eq. (35). In turn, $\kappa_{\mu_a}(\mathbf{q}_s,\mathbf{q}_d;x)$ is expressed in terms of the functions $g(\mathbf{q};x,\hat{\mathbf{s}};x',\hat{\mathbf{s}}')$, Eq. (144), as

$$\kappa_{\mu_a}(\mathbf{q}_s,\mathbf{q}_d;x) = \int g(\mathbf{q}_s;x_s,\hat{\mathbf{x}};x,\hat{\mathbf{s}}) g(\mathbf{q}_d;x,\hat{\mathbf{s}};x_d,\hat{\mathbf{x}}) d^2s. \tag{145}$$

The angular integral in Eq. (145) can be evaluated with the use of

$$\int \frac{d^2s}{(\mu_t - i\mathbf{q}_1\cdot\hat{\mathbf{s}})(\mu_t - i\mathbf{q}_2\cdot\hat{\mathbf{s}})} = \frac{4\pi}{\sqrt{(\mathbf{q}_1\times\mathbf{q}_2)^2 + \mu_t^2(\mathbf{q}_1-\mathbf{q}_2)^2}} \times \left[\arctan\frac{\sqrt{(\mathbf{q}_1\times\mathbf{q}_2)^2 + \mu_t^2(\mathbf{q}_1-\mathbf{q}_2)^2}}{\mathbf{q}_1\cdot\mathbf{q}_2 + \mu_t^2} + \pi\Theta(-\mathbf{q}_1\cdot\mathbf{q}_2 - \mu_t^2) \right], \tag{146}$$

where $\Theta(x)$ is the step function.

VII. SUMMARY

We have presented a general theoretical framework for image reconstruction methods in optical diffusion tomogra-

phy. These methods require that the data are measured on surfaces with translational or rorational invariance with respect to one or more generalized coordinates. This approach can have the effect of dramatically improving computational efficiency, allowing the use of extremely large data sets.

It should be noted that the family of image reconstruction methods described in this paper is only applicable to regular measurement geometries, such as the slab or cylinder. Problems involving irregular boundaries or boundaries with complicated shape cannot be treated using these methods. Such problems should be solved by means of numerical methods. Unfortunately, these methods preclude the treatment of large data sets (more than 10^3–10^4 data points) due to high computational complexity.

If, however, the boundaries are relatively simple, taking account of translational invariance leads to a reduction in computational complexity. In particular, it allows the replacement of the problem of diagonalizing a matrix of size N_1N_2 where N_1 is the number of "external" degrees of freedom and N_2 the number of "internal" degrees of freedom to the problem of diagonalizing N_1 matrices of size N_2 each. The computational complexity of the second problem is smaller by a factor of N_1^2. In many problems, N_1 is the number of sources used to illuminate the medium. For example, if the sources are located on a 100×100 lattice, the computational complexity is smaller by a factor of 10^8. The possibility of utilizing extremely large data sets suggests that the highest possible spatial resolution can be achieved in simple measurement geometries.

We have also presented the theory of multiprojection ODT where all data are treated self-consistently. An SVD pseudoinverse is obtained with all symmetries intrinsic to the multiprojection measurement scheme. It is expected that multiple projections can further improve image quality due to the mutual interchange of the "depth" and "transverse" directions.

ACKNOWLEDGMENTS

This work was supported by the AFOSR and NIH. The authors are grateful to Dr. George Panasyuk for useful discussions.

APPENDIX: INVERSION FORMULAS FOR THE PLANAR GEOMETRY WITH ROTATIONS WHEN THE y_s VARIABLE IS NOT ON A LATTICE

An approach to treating the variable y_s alternative to the one used in Sec. IV can be adopted. Namely, assume that y_s is not sampled on a lattice, but is in some finite set. Then we can view y_s as another "internal variable" and perform integration over dq_y in Eq. (85) to obtain

$$\Gamma(\mu,y_s,z_s,\theta;\varphi,z,R) = \sum_{m=-\infty}^{\infty}\int\frac{dq_s}{(2\pi)^2}A(\mu,y_s,q_z,m;R)\times\exp[im(\varphi-\theta)+iq_z(z-z_s)], \tag{A1}$$

where

$$A(\mu,y_s,q_z,m;R)=\int\frac{dq_y}{2\pi}a(\mu,q_y,q_z,m;R)\exp(-iq_yy_s). \tag{A2}$$

Since no translational invariance in the direction y is present, it is logical to include y_s in the list of "internal" variables and write $\mu=(\omega,\Delta\boldsymbol{\rho},y_s)$. Then Eq. (A1) can be compactly rewritten as

$$\Gamma(\mu,z_s,\theta;\varphi,z,R)=\sum_{m=-\infty}^{\infty}\int\frac{dq}{(2\pi)^2}A(\mu,q,m;R)\times\exp[im(\varphi-\theta)+iq(z-z_s)]. \tag{A3}$$

But this expansion has exactly the same form as the expansion of the kernel Γ, Eq. (100) , which was obtained in cylindrical geometry with the only distinction that $A(\mu,q,m;R)$ in Eq. (A3) is replaced by $K(\mu,q,m;R)$ in Eq. (100) and the list of "internal" variables collected in μ is different in these two cases. Nevertheless, it is straightforward to show that the reconstruction formulas (102)–(106) obtained in cylindrical geometry apply in the case of a rotated geometry with the substitution $K\to A$. It should be kept in mind that the functions K and A are different since they are obtained by different transformations of respective functions κ. The latter are also different in the planar and cylindrical cases, as discussed in Sec. VI.

[1] *Medical Optical Tomography: Functional Imaging and Monitoring*, edited by G. Mueller (SPIE, Bellingham, WA, 1993).
[2] *Proceedings of Optical Tomography and Spectroscopy of Tissue*, edited by B. Chance and R. Alfano (SPIE, Bellingham, WA, 1995).
[3] *Proceedings of Optical Tomography and Spectroscopy of Tissue II*, edited by B. Chance and R. Alfano (SPIE, Bellingham, WA, 1997).
[4] *Proceedings of Optical Tomography and Spectroscopy of Tissue III*, edited by B. Chance, R. Alfano, and B. Tromberg (SPIE, Bellingham, WA, 1999).
[5] *Proceedings of Optical Tomography and Spectroscopy of Tissue*, edited by B. Chance, R. Alfano, B. Tromberg, M. Tamura, and E. M. Sevick-Muraca (SPIE, Bellingham, WA, 2001).
[6] A. Ishimaru, *Wave Propagation and Scattering in Random Media* (Academic, San Diego, 1978).
[7] M. C. W. van Rossum and T. M. Nieuwenhuizen, Rev. Mod. Phys. **71**, 313 (1999).
[8] S. R. Arridge, Inverse Probl. **15**, R41 (1999).
[9] J. Schotland and J. Leigh, FASEB J. **61**, 446 (1992).
[10] J. C. Schotland and V. A. Markel, J. Opt. Soc. Am. A **18**, 2767 (2001).

[11] V. A. Markel and J. C. Schotland, Phys. Rev. E **64**, 035601(R) (2001).
[12] V. A. Markel and J. C. Schotland, Appl. Phys. Lett. **81**, 1180 (2002).
[13] V. A. Markel and J. C. Schotland, Opt. Lett. **27**, 1123 (2002).
[14] V. A. Markel and J. C. Schotland, J. Opt. Soc. Am. A **20**, 890 (2003).
[15] K. M. Case and P. F. Zweifel, *Linear Transport Theory* (Addison-Wesley, Reading, MA, 1967).
[16] R. Aronson, J. Opt. Soc. Am. A **12**, 2532 (1995).
[17] M. V. Berry and I. C. Percival, Opt. Acta **33**, 577 (1986).
[18] In Sec. IV we will also use a cylindical coordinate system in which $\mathbf{r}=(\varphi,z,R)$ where $x=R\cos\varphi$, $y=R\sin\varphi$ and z is not transformed.
[19] P. S. Carney, V. A. Markel, and J. C. Schotland, Phys. Rev. Lett. **86**, 5874 (2001).
[20] M. Xu, M. Lax, and R. R. Alfano, J. Opt. Soc. Am. A **18**, 1535 (2001).
[21] V. A. Markel and J. C. Schotland, J. Opt. Soc. Am. A **19**, 558 (2002).
[22] L. A. Apresyan and Y. A. Kravtsov, *Radiation Transfer: Statistical and Wave Aspects* (Gordon and Breach, Amsterdam, 1996).